Nuclear Instruments and Methods in Physics Research A 600 (2009) 568–593

Contents lists available at ScienceDirect

Nuclear Instruments and Methods in Physics Research A

journal homepage: www.elsevier.com/locate/nima

The Borexino detector at the Laboratori Nazionali del Gran Sasso

G. Alimonti [a], C. Arpesella [1], H. Back [c], M. Balata [b], D. Bartolomei [d], A. de Bellefon [e], G. Bellini [a], J. Benziger [f], A. Bevilacqua [g], D. Bondi [g], S. Bonetti [a], A. Brigatti [a], B. Caccianiga [a], L. Cadonati [d], F. Calaprice [d], C. Carraro [g], G. Cecchet [h], R. Cereseto [g], A. Chavarria [d], M. Chen [d], A. Chepurnov [i], A. Cubaiu [b], W. Czech [k], D. D'Angelo [a,k], F. Dalnoki-Veress [d], A. De Bari [h], E. De Haas [d], A. Derbin [l], M. Deutsch [1], A. Di Credico [b], A. Di Ludovico [d], G. Di Pietro [b], R. Eisenstein [d], F. Elisei [s], A. Etenko [m], F. von Feilitzsch [k], R. Fernholz [d], K. Fomenko [n], R. Ford [b,d,a], D. Franco [a,o], B. Freudiger [1], N. Gaertner [k], C. Galbiati [a,d], F. Gatti [g], S. Gazzana [b], V. Gehman [c], M. Giammarchi [a], D. Giugni [a], M. Goeger-Neff [k], T. Goldbrunner [k], A. Golubchikov [m,a], A. Goretti [a,b,d], C. Grieb [k,c], C. Hagner [k], T. Hagner [k], W. Hampel [o], E. Harding [d], S. Hardy [c], F.X. Hartmann [o], R. von Hentig [k], T. Hertrich [k], G. Heusser [o], M. Hult [j], A. Ianni [b], An. Ianni [d], L. Ioannucci [b], K. Jaenner [o], M. Joyce [c], H. de Kerret [e], S. Kidner [c], J. Kiko [o], T. Kirsten [o], V. Kobychev [r], G. Korga [b], G. Korschinek [k], Yu. Kozlov [m], D. Kryn [e], P. La Marche [b,d], V. Lagomarsino [g], M. Laubenstein [b], C. Lendvai [k], M. Leung [d], T. Lewke [k], E. Litvinovich [m], B. Loer [d], F. Loeser [d], P. Lombardi [a], L. Ludhova [a], I. Machulin [m], S. Malvezzi [a], A. Manco [g], J. Maneira [a], W. Maneschg [o], I. Manno [a,p], D. Manuzio [g], G. Manuzio [g], M. Marchelli [g], A. Martemianov [1], F. Masetti [s], U. Mazzucato [s], K. McCarty [d], D. McKinsey [d], Q. Meindl [k], E. Meroni [a], L. Miramonti [a], M. Misiaszek [q], D. Montanari [b], M.E. Monzani [a], V. Muratova [l], P. Musico [g], H. Neder [o], A. Nelson [d], L. Niedermeier [k], S. Nisi [b], L. Oberauer [k], M. Obolensky [e], M. Orsini [b], F. Ortica [s], M. Pallavicini [g,*], L. Papp [b], R. Parcells [d], S. Parmeggiano [a], M. Parodi [g], N. Pelliccia [s], L. Perasso [a], A. Pocar [d], R. Raghavan [c], G. Ranucci [a], W. Rau [o,b], A. Razeto [g,b], E. Resconi [a,g], P. Risso [g], A. Romani [s], D. Rountree [c], A. Sabelnikov [m], P. Saggese [a], R. Saldhana [d], C. Salvo [g], R. Scardaoni [a], D. Schimizzi [d], S. Schönert [o], K.H. Schubeck [k], T. Shutt [d], F. Siccardi [g], H. Simgen [o], M. Skorokhvatov [m], O. Smirnov [n], A. Sonnenschein [d], F. Soricelli [b], A. Sotnikov [n], S. Sukhotin [m], C. Sule [d], Y. Suvorov [a,m], V. Tarasenkov [m], R. Tartaglia [b], G. Testera [g], D. Vignaud [e], S. Vitale [1], R.B. Vogelaar [d,c], V. Vyrodov [m], B. Williams [c], M. Wojcik [q], R. Wordel [j], M. Wurm [k], O. Zaimidoroga [n], S. Zavatarelli [g], G. Zuzel [q,o], Borexino Collaboration

[a] Dipartimento di Fisica, Universitá di Milano and INFN Milano, via Celoria 16, I-20133 Milano, Italy
[b] Laboratori Nazionali del Gran Sasso, SS 17bis Km 18+910, I-67010 Assergi (AQ), Italy
[c] Physics Department, Robeson Hall, Virginia Polytechnic Institute and State University, Blacksburg, VA 24061-0435, USA
[d] Department of Physics, Princeton University, Jadwin Hall, Washington Road, Princeton, NJ 08544-0708, USA
[e] Astroparticule et Cosmologie APC, 10 rue Alice Domon et Léonie Duquet, 75205 Paris Cedex 13, France
[f] Department of Chemical Engineering, Princeton University, Engineering Quadrangle, Princeton, NJ 08544-5263, USA
[g] Dipartimento di Fisica, Universitá di Genova and INFN Genova, via Dodecaneso 33, I-16146 Genova, Italy
[h] Dipartimento di Fisica, Universitá di Pavia and INFN Pavia, via Bassi 6, I-27100 Pavia, Italy
[i] Moscow University, Moscow, Russia
[j] EC-JRC-IRMM, Retieseweg 111, 2440 Geel, Belgium
[k] Technische Universität München, James Franck Strasse E15, D-85747 Garching, Germany
[l] St. Petersburg Nuclear Physics Institute, Gatchina, Russia
[m] RRC Kurchatov Institute, Kurchatov Sq. 1, 123182 Moscow, Russia
[n] J.I.N.R., Joliot Curie str. 6, 141980 Dubna (Moscow Region), Russia
[o] Max-Planck-Institut für Kernphysik, Postfach 103 980, D-69029 Heidelberg, Germany
[p] KFKI-RMKI, 1121 Budapest, Hungary
[q] Institute of Physics, Jagellonian University, ul. Reymonta 4, PL-30059 Krakow, Poland
[r] Institute for Nuclear Research, MSP 03680 Kiev, Ukraine
[s] Dipartimento di Chimica, Universitá di Perugia and INFN Perugia, via Elce di Sotto 8, I-06123 Perugia, Italy

*For more information, please contact: Tel.: +39 010 3536661; fax: +39 010 313358.
E-mail address: marco.pallavicini@ge.infn.it (M. Pallavicini).
[1] Deceased.

0168-9002/$ - see front matter
doi:10.1016/j.nima.2008.11.076

ARTICLE INFO

Article history:
Received 24 June 2008
Received in revised form
25 October 2008
Accepted 7 November 2008
Available online 30 November 2008

Keywords:
Solar neutrino
Low background detectors
Liquid scintillators

ABSTRACT

Borexino, a large volume detector for low energy neutrino spectroscopy, is currently running underground at the Laboratori Nazionali del Gran Sasso, Italy. The main goal of the experiment is the real-time measurement of sub-MeV solar neutrinos, and particularly of the monoenergetic (862 keV) ^{7}Be electron capture neutrinos, via neutrino–electron scattering in an ultra-pure liquid scintillator. This paper is mostly devoted to the description of the detector structure, the photomultipliers, the electronics, and the trigger and calibration systems. The real performance of the detector, which always meets, and sometimes exceeds, design expectations, is also shown. Some important aspects of the Borexino project, i.e. the fluid handling plants, the purification techniques and the filling procedures, are not covered in this paper and are, or will be, published elsewhere (see Introduction and Bibliography).

1. Introduction

Borexino is a large volume liquid scintillator detector whose primary purpose is the real-time measurement of low energy solar neutrinos. It is located deep underground ($\simeq$ 3800 m of water equivalent, m w.e.) in the Hall C of the Laboratori Nazionali del Gran Sasso (Italy), where the muon flux is suppressed by a factor of $\approx 10^{6}$.

The main goal of the experiment is the detection of the monochromatic neutrinos that are emitted in the electron capture decay of ^{7}Be in the Sun [1]. This measurement is now in progress, and the very first results have been already published in Ref. [2]. However, as shown there, the observed radioactive background is much lower than expected, which results in a potential broadening of the scientific scope of the experiment. Particularly, Borexino now also aims at the spectral study of other solar neutrino components, such as the CNO, pep [3] and, possibly, pp and ^{8}B neutrinos.

Besides solar physics, the unprecedented characteristics of its apparatus make Borexino very competitive in the detection of anti-neutrinos ($\bar{\nu}$), particularly those of geophysical origin. The physics goals of the experiment also include the detection of a nearby supernova, the measurement of the neutrino magnetic moment by means of a powerful neutrino source, and the search for very rare events like the electron decay [4] or the nucleon decay into invisible channels [5].

In Borexino low energy neutrinos (ν) of all flavors are detected by means of their elastic scattering of electrons or, in the case of electron anti-neutrinos, by means of their inverse beta decay on protons or carbon nuclei. The electron (positron) recoil energy is converted into scintillation light which is then collected by a set of photomultipliers (PMTs).

This technique has several advantages over both the water Cherenkov detectors and the radiochemical detectors used so far in solar neutrino experiments. Water Cherenkov detectors, in fact, cannot effectively detect solar neutrinos whose energy is below 6 MeV, both because the Cherenkov light yield is low and because the intrinsic radioactive background cannot be pushed down to sufficiently low levels. On the other hand, radiochemical experiments cannot intrinsically perform spectral measurements and do not detect events in real time.

An organic liquid scintillator solves the aforementioned problems: the low energy neutrino detection is possible because of the high light yield that in principle allows the energy threshold to be set down to a level of a few tens of keV[2]; the organic nature of the scintillator, and its liquid form at ambient temperature, provide very low solubility of ions and metal impurities, and yield the technical possibility to purify the material as required. However, no measurement of the direction of the incoming neutrino is possible and, even more importantly, the neutrino induced events are intrinsically indistinguishable from β and γ radioactivity, posing formidable requirements in terms of radiopurity of the scintillator and of the detector materials.

According to the Standard Solar Model,[3] the order of magnitude of sub-MeV solar neutrino interactions rate is a few tens counts/day for about 100 ton of target material and with an energy threshold of 200 keV. This rate corresponds to an equivalent activity of a few $\times 10^{-9}$ Bq/kg. If one compares this low number with the typical radioactivity of materials (drinking water $\simeq$ 10 Bq/kg, air $\simeq$ 10 Bq/kg, rock $\simeq$ 100–1000 Bq/kg) it is immediately apparent that the core of the Borexino detector must be 9–10 orders of magnitude less radioactive than anything on Earth. Typical radioactive contaminants in solid materials and water are ^{238}U and ^{232}Th daughters, and ^{40}K. Air and therefore normally also commercially available nitrogen are typically contaminated by noble gases like ^{222}Rn, ^{39}Ar and ^{85}Kr.

The necessity to measure such a low neutrino flux with a massive detector poses severe requirements in terms of radiopurity, not only for the scintillator itself, but also for the surrounding materials. Additionally, the neutrino target (100 ton of "fiducial volume" in Borexino) must be almost completely shielded from external γ radiation and neutrons originating from the rock and from the detector materials.

For almost 20 years the Borexino collaboration has been addressing this problem by developing suitable purification techniques for scintillator, water, and nitrogen, by performing careful material selections, by developing innovative cleaning techniques for metal surfaces, and by building and operating a prototype of the Borexino detector, the Counting Test Facility (CTF). In particular, CTF has played a crucial role in this long R&D phase. It is still the only instrument available in the world (except Borexino itself) with the sensitivity to measure the radioactive contamination of a liquid scintillator down to levels as low as 10^{-16} g/g in ^{238}U and ^{232}Th.[4] For more details about the specific requirements in terms of radiopurity of the scintillator and of the detector materials for solar neutrino measurement in Borexino see Refs. [1,6]. For the reader's convenience, we summarize here the main requirements:

- The internal radioactivity of the scintillator must be low enough compared to the expected neutrino signal. Particularly,

[2] However, the unavoidable contamination of ^{14}C that is present in any organic liquid practically limits the "neutrino window" above $\approx$ 200 keV.

[3] Regardless of neutrino oscillations which are not relevant at this point.

[4] Here and everywhere in this paper the unit g/g stands for 1 g of contamination per gram of solution or material.

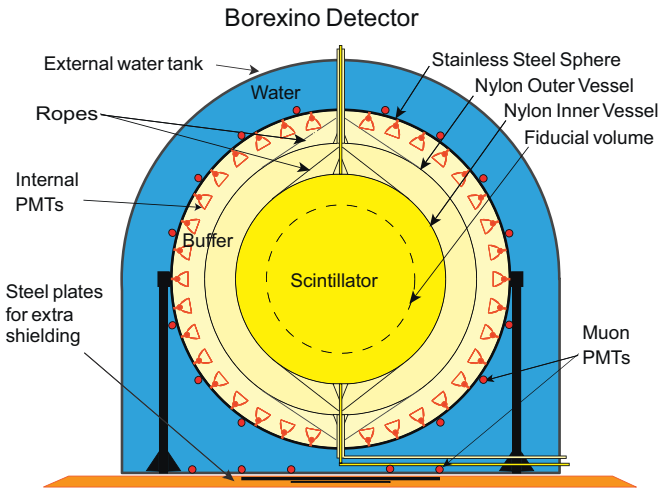

Fig. 1. Schematic drawing of the Borexino detector.

the design goal was $<10^{-16}$ g/g in ^{238}U and ^{232}Th, $<10^{-14}$ g/g in K_{nat}.[5]

- The scintillator must be thoroughly sparged with nitrogen gas in order to remove oxygen (which may deteriorate the optical properties of the scintillator) and air borne contaminants (radioactive). The nitrogen purity requirement is such that the expected background from ^{222}Rn, ^{39}Ar and ^{85}Kr in 100 ton of target scintillator must be less than 1 count/day. This corresponds to 0.36 ppm for Ar and 0.16 ppt for Kr.
- The total amount of external γ radiation penetrating the central part of the scintillation volume should be below 1 count/day in 100 ton. This puts stringent requirements on all materials surrounding the detector, the requirements being more and more stringent for materials closer to the center.

This paper is devoted to the description of the Borexino detector. It is not intended to be a complete reference of the Borexino scientific goals, nor will it provide a comprehensive description of the experiment as a whole. The focus here is the detector, defined as the collection of scintillator volume, containment vessels, light detection devices (PMTs and electronics), data acquisition, and calibration systems. We do not cover here the purification plants (a very large fraction of the Borexino equipment) nor the purification techniques adopted to purify scintillator, water and nitrogen. Also, the filling procedures are not covered in this paper. All these very important parts of the experiment are either already published or will be published in the near future.

The paper is structured as follows: Section 2 gives a general description of the detector; Section 3 summarizes the main scintillator features; Section 4 describes the inner nylon vessels which contain the scintillator and act as ultimate barriers against external contaminations; Section 5 describes the main detector with its PMTs, front end electronics, and data acquisition electronics; Section 6 describes the muon detector; Sections 7 and 8 describe the trigger and the data acquisition systems; Sections 9 and 10 describe the laser based calibration systems for the PMTs and for the monitoring of the scintillator transparency; Section 11 describes the insertion system for source calibrations. Finally, the last section provides a brief overview of the detector performance on real data. For more details about detector performance see Refs. [2,7].

[5] K_{nat} is potassium in its natural isotopic abundance.

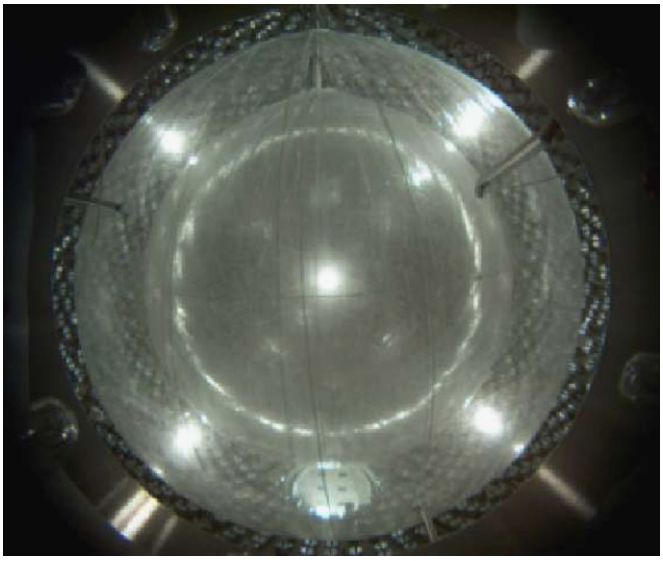

Fig. 2. The inner and outer nylon vessels installed and inflated with nitrogen in the Stainless Steel Sphere.

2. General description of the Borexino detector

Borexino is a liquid scintillator detector designed to provide the largest possible fiducial volume of ultra-clean scintillator [1,6].

The detector is schematically depicted in Fig. 1. The inner part is an unsegmented Stainless Steel Sphere (SSS) that is both the container of the scintillator and the mechanical support of the PMTs. Within this sphere, two nylon vessels separate the scintillator volume in three shells of radii 4.25, 5.50 and 6.85 m, the latter being the radius of the SSS itself. The inner nylon vessel (IV) contains the liquid scintillator solution, namely PC (pseudocumene, 1,2,4-trimethylbenzene $C_6H_3(CH_3)_3$) as a solvent and the fluor PPO (2,5-diphenyloxazole, $C_{15}H_{11}NO$) as a solute at a concentration of 1.5 g/l (0.17% by weight). The second and the third shell contain PC with a small amount (5 g/l) of DMP (dimethylphthalate, $C_6H_4(COOCH_3)_2$) that is added as a light quencher in order to further reduce the scintillation yield of pure PC [8].

The PC/PPO solution that we adopted as liquid scintillator satisfies specific requirements: high scintillation yield ($\approx 10^4$ photons/MeV), high light transparency (the mean free path is typically 8 m) and fast decay time (≈ 3 ns), all essential for good energy resolution, precise spatial reconstruction, and good discrimination between β-like events and events due α particles.[6]

Furthermore, several conventional petrochemical techniques are feasible to purify the hundred of tons of fluids needed by Borexino. The feasibility of reaching the level of radiopurity required by Borexino was first proven in the tests performed in the CTF in 1996 [9,10]. Although pure PC is a scintillator itself, the addition of a small quantity of PPO greatly improves the time response and shifts the emission wavelength spectrum to higher values, thus better matching the PMT efficiency window.

[6] The time profile of the emitted light in an organic scintillator is usually different for β-like events and α particles.

The Inner Vessel (IV) is made of 125 μm thick Nylon-6 carefully selected and handled in order to achieve maximum radiopurity [11]. Since the PC/PPO solution is slightly lighter (about 0.4%) than the PC/DMP solution, the IV is anchored to the bottom (south pole of the SSS) with a set of nylon strings. The outer nylon vessel (OV) has a diameter of 11 m and is built with the same material as the inner one. The OV is a barrier that prevents ^{222}Rn emanated from the external materials (steel, glass, PMT materials) to diffuse into the fiducial volume. Fig. 2 shows the two nylon vessels inflated in the SSS immediately after their installation.

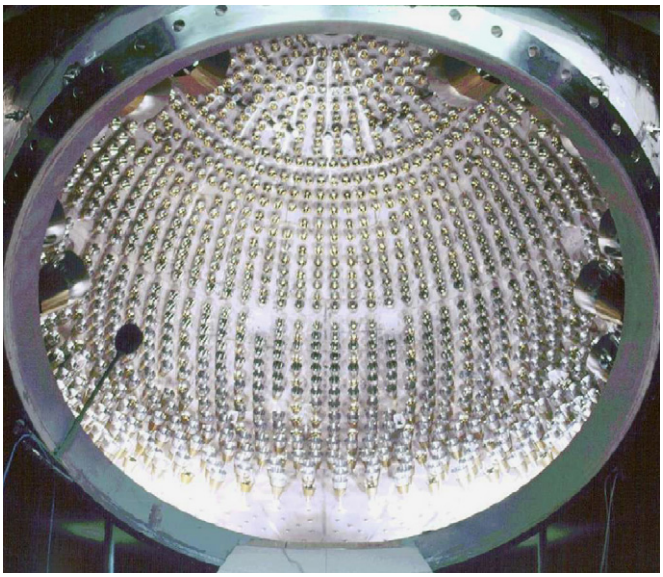

Fig. 3. Inner surface of the Stainless Steel Sphere. The picture is taken from the main SSS door, and shows the internal surface of the sphere with PMTs evenly mounted inside. The total number of PMTs is 2212.

The buffer fluid between the inner nylon vessel and the SSS (PC/DMP solution) is the last shielding against external backgrounds. The use of PC as a buffer is convenient because it matches both the density and the refractive index of the scintillator, thus reducing the buoyancy force for the nylon vessel and avoiding optics aberrations that would spoil the spatial resolution.

The addition of the DMP quenches the scintillation yield of the buffer fluid by a factor of 20. This is important in order to avoid the unacceptable trigger rate due to the radioactivity of the PMTs.

The scintillation light is collected by 2212 PMTs that are uniformly attached to the inner surface of the SSS (see Fig. 3). All but 384 PMTs are equipped with light concentrators that are designed to reject photons not coming from the active scintillator volume, thus reducing the background due to radioactive decays originating in the buffer liquid or γ's from the PMTs. The 384 PMTs without concentrators can be used to study this background, and to help identify muons that cross the buffer, but not the IV. The details of the PMT design are described in Section 5.1.

The SSS is supported by 20 steel legs and enclosed within a large tank that is filled with ultra-pure water.

The tank (see Fig. 4) has a cylindrical base with a diameter of 18 m and a hemispherical top with a maximum height of 16.9 m.

The Water Tank (WT) is a powerful shielding against external background (γ rays and neutrons from the rock) and is also used

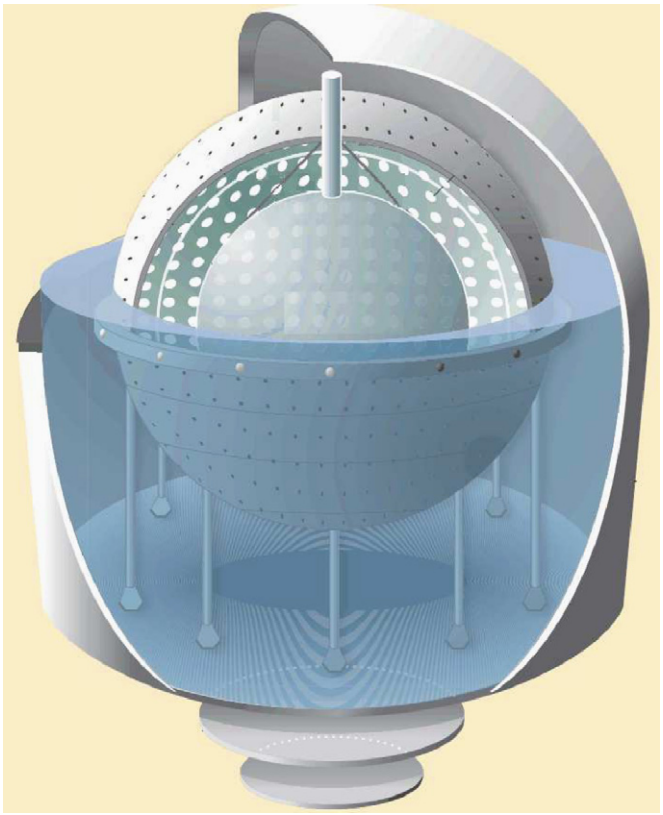

Fig. 4. A pictorial drawing of the Borexino detector. Inside the Water Tank, the stainless steel sphere is supported by 20 steel legs. Within the sphere, the drawings shows some PMTs (white full circles) and the inner and outer nylon vessels. The steel plates beneath the tank improve the shielding against radiation from the rock.

Fig. 5. The inner surface of the Water Tank covered with a layer of Tyvek. The Tyvek sheets improve light collection in the outer detector by reflecting the photons back into the water.

as a Cherenkov muon counter and muon tracker. The muon flux, although reduced by a factor of 10^6 by the 3800 m w.e. depth of the Gran Sasso Laboratory, is of the order of $1\,m^{-2}\,h^{-1}$, corresponding to about 4000 muons per day crossing the detector. This flux is well above Borexino requirements and a strong additional reduction factor (about 10^4) is necessary. Therefore the WT is equipped with 208 PMTs that collect the Cherenkov light emitted by muons in water. In order to maximize the light collection efficiency the SSS and the interior of the WT surface are covered with a layer of Tyvek, a white paper-like material made of polyethylene fibers (see Fig. 5).

3. The scintillator

The choice of the scintillator mixture was performed taking into account both its optical properties and the radiopurity constraints dictated by the experiment physics goals. The scintillator optical properties have been widely studied on small and medium scale samples by using both ultra-violet light as well as α, β and γ radiation [12,13]. These measurements allowed for the comparison of the main characteristics of different scintillators (emission spectrum, time response, light yield, α/β discrimination capability) in order to select the most suitable one for Borexino [13].

The final test of a large scale sample of the selected scintillator mixture was performed in the Borexino prototype CTF (4 ton of PC + PPO in a spherical vessel viewed by 100 PMTs). Due to the large size and 4π sensitivity of the apparatus, the CTF test made it possible to single out and quantify the effect of processes like absorption and re-emission off the fluor (PPO) and scattering on the solvent (pseudocumene). These phenomena were found to have a significant impact on the overall performance of the detector. In particular, the energy and position resolution were most severely affected [14]. The energy resolution critically relies on the high light yield and low auto-absorption of the scintillator, as well as having an optimal match between the emitted light spectrum and the PMT quantum efficiency. The PC + PPO mixture has a light yield of ≃ 10 000 photons/MeV and its emission spectrum peaks at 360 nm (see Fig. 6) thus matching well the phototube peak efficiency. This fact, together with the low absorption of the scintillator[7] and buffer fluid (see Fig. 7) leads to an overall light collection of ≃ 500 photons/MeV of deposited energy, corresponding to a resolution (1σ) of ≃ 5% at 1 MeV. The time response of the scintillator is also critical: in particular, a fast response is needed to achieve good position resolution, while α/β discrimination relies on the different shapes of the photon time distribution for α and β events. The time response of the PC + PPO mixture chosen for Borexino was measured on a small sample of scintillator and is shown in Fig. 8 for both α and β particles: the curves can be phenomenologically described as the sum of several exponentials having time constants τ_i. The first exponential (corresponding to the fastest time decay) accounts for most of the emitted light (90% in the case of βs and 65% in the case of αs) and has $\tau = 3.5$ ns (only a factor 2 larger than the intrinsic PPO time decay). The difference in the amount of light emitted at longer times (10% in the case of β's and 35% in the case of α's) is crucial for the effectiveness of pulse-shape discrimination techniques. See Refs. [15,16,50] for details.

[7] It should also be noted that whenever a photon is absorbed by PPO it has a high probability (80%) to be re-emitted with a random direction and with the typical PPO emission spectrum and decay time (1.6 ns). Therefore, in most cases the photon is not lost, but effectively "slowed down".

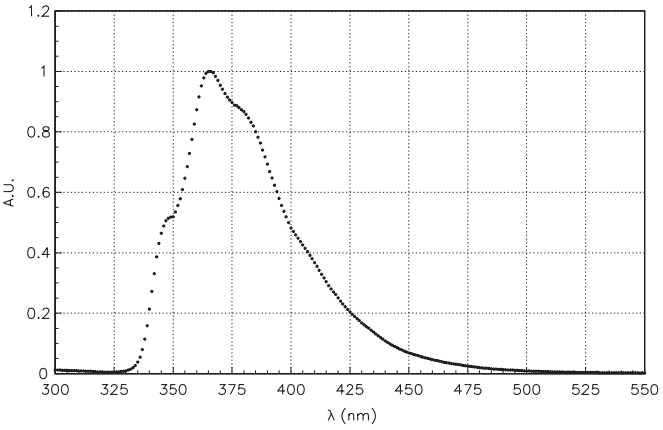

Fig. 6. Emission spectrum of the PC + PPO mixture used in Borexino.

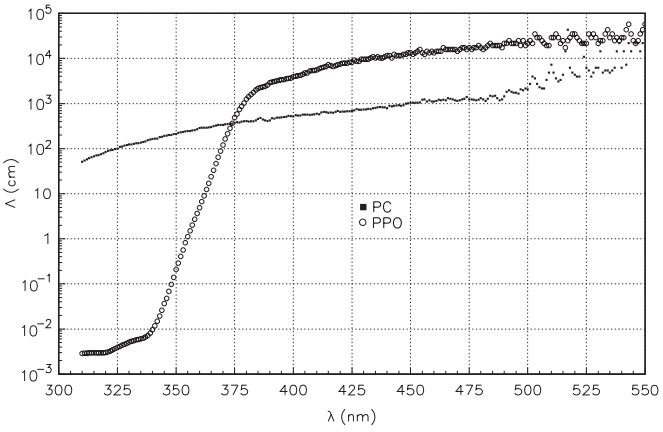

Fig. 7. Attenuation length of PC (full squares) and PPO (empty circles).

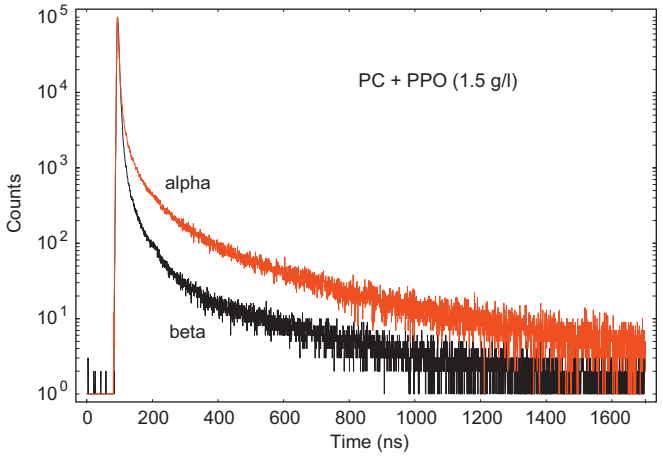

Fig. 8. Time response of the Borexino scintillator mixture for α and β particles.

4. The nylon vessels

The design of the Borexino scintillator containment system is a coherent part of the general strategy to keep a large volume of scintillator in place while minimizing the radioactive background from the materials in contact with it. As described in Section 2, Borexino exploits a heavy mechanical component, the 6.85 m radius SSS, both for the support of large buoyant forces due to the need for an external water shield, and also to act as a support

structure for the PMTs. (The dual use of the SSS for scintillator containment and for PMT support is made possible by the steel having lower radioactivity than the PMTs.)

In the Borexino design, the SSS and the PMTs are kept as far as possible from the active scintillator by an intermediate volume of non-scintillating buffer fluid, in order to reduce the background from gamma rays. With the SSS carrying the heavy structural loads, the vessel that separates the scintillator and the inert buffer can be a low-mass, relatively delicate membrane made from a material chosen primarily for its properties of optical clarity, chemical compatibility with PC and low intrinsic radioactivity.

The design chosen for the scintillator containment vessel is a thin-walled (0.125 mm thick), transparent nylon balloon, 4.25 m in radius, held in place at the center of the SSS. Nylon has approximately the same index of refraction (1.53) as PC, and thin nylon sheets can be made to be very transparent. It is chemically compatible with both the scintillator (PC + PPO) within this vessel, and the passive buffer fluid (PC + DMP) outside it. Nylon also retains its material strength even while immersed in cold water (as during the water filling stage of the detector commissioning) for many months. In order to prevent the quenching compound (DMP) from leaking into the active scintillator, or the fluor (PPO) from leaking into the passive buffer volume, the scintillator containment vessel must also be sufficiently leak-tight, to better than 0.01 cm^3/s liquid leak at a pressure difference of 1 mbar. This should be compared with a measured value of 0.005 cm^3/s [11].

To prevent contamination from the long-lived ^{210}Pb radon daughter, the vessel was constructed inside the Princeton University clean room, which was kept low in radon by a dedicated pressure-swing adsorption system [17]. The ability to assemble the vessel off-site, under very stringent clean-room conditions, is an additional advantage of the thin nylon membrane design. The Nylon-6 used in the vessel is a blend of Sniamid ADS40T and Ultramid B4, specially extruded at the mf-folien plant in Germany. It is sufficiently radiopure, having a ^{226}Ra activity of <21 mBq/kg [18] that it was expected to contribute fewer than seven decays per day of ^{222}Rn within the Borexino fiducial volume [19], and in fact contributes fewer than two [2]. The rate of gamma rays within the fiducial volume due to the nylon film of the vessel is thought to be much less than a single event per day [11].

The scintillator containment vessel (IV) is completely surrounded by a second, larger Nylon-6 membrane (Outer Vessel, OV) in order to square the effectiveness of the system as a barrier against radon atoms diffusing inward from outer parts of the detector. The two vessels were pre-assembled in this nested condition even before being shipped to Gran Sasso for installation and inflation to their final spherical shapes. The OV, 5.5 m in radius, divides the passive buffer volume into two concentric parts. As it is not in close contact with the scintillator fluid, its requirements for radiopurity and leak tightness are lower; the measured values of 0.21 ± 0.3 mBq/kg of ^{226}Ra, and 0.1 cm^3/s (liquid leak) at 1 mbar ΔP, respectively, are more than adequate [11,18].

The nylon membranes of both vessels have the material strength (a yield point of 20–70 MPa, depending on ambient water content) to survive the forces due to the 0.4% density difference between the active scintillator and passive buffer fluids. They were even designed to withstand a 5 °C temperature gradient (which would cause an additional 0.5% density difference) for short time periods. However, because their material is flexible, the vessels must be held in place by a support structure. Each nylon sphere is attached to a vertically oriented cylindrical "end region" at both top and bottom. For the IV end regions, very radiopure materials (cast nylon and copper) were chosen at the expense of some material strength, while stainless steel was used for the OV end regions; these contribute the largest fraction of the roughly two gamma events per day in the fiducial volume coming from the vessel support structures and instrumentation. Each IV end region is bolted to the inner end of the corresponding OV end region, which in turn is fixed rigidly in place to top or bottom of the SSS. To keep the vessels constrained in roughly spherical shapes, more than just two fixed attachment points are needed: each vessel is also held in place by two sets of ropes (one set attaching at each end region) that loop vertically over and under them. A third set of ropes goes around each vessel horizontally, completing a coarse mesh. All ropes are made of Tensylon, an ultra high density polyethylene (UHDPE). Though Tensylon is not perfect from a material strength standpoint, it is essentially free of potassium (including ^{40}K, a naturally occurring gamma ray emitter), unlike most common rope materials.

The end regions are outfitted with sets of instrumentation for monitoring the detector. These include strain gauges that hold the rope ends to the end regions, for monitoring the vessels' buoyancy, temperature sensors in the buffer volumes, differential pressure gauges, and a set of optical fibers. The fibers are routed to small PTFE diffuser bulbs fixed at various points on the vessel outer surfaces [20]. These bulbs may be lit up with laser light for use in monitoring the shapes and positions of the vessels with the internal camera system, as well as for calibrating the position reconstruction algorithms used in analyzing experimental data acquired with the detector electronics. Each end region also permits the passage of fluid into the corresponding detector volume for filling and drainage operations.

More detailed information on the Borexino nylon vessels, their fabrication and design, and the associated support structures and instrumentation, is available in Refs. [11,20–22].

5. The inner detector

As we summarized in Section 2, there are two main detection systems in Borexino: the inner detector, composed of 2212 PMTs collecting the scintillation light inside the SSS and the outer detector (OD), composed of 208 PMTs that detect the Cherenkov light produced by muons in water. In this section we describe the inner detector, focussing on PMTs design, front-end and read-out electronics. Other details concerning the mechanical structure of the Borexino inner detector can be found elsewhere [1,11,20,21,23–25]. The section is structured as follows: in Section 5.1 we report the main characteristics of the inner detector PMTs and their PC-proof sealing, while Section 5.2 describes the inner detector front-end and read-out electronics.

5.1. The inner detector PMTs

The necessity to measure the energy of each scintillation event and to reconstruct its position by means of a time of flight technique put severe constraints on the selection of the best PMT for Borexino.

Monte Carlo simulations showed that the mean number of photoelectrons (p.e.) detected by one PMT are $0.02-2.0$ for events with energy between 250–800 keV. It is therefore important that the PMTs have a good single electron charge resolution in order to get an accurate reconstruction of the event energy. The interaction point in the detector is reconstructed using the time information from the PMTs. The position resolution depends therefore on the precision of the measurement of the arrival time of a single p.e. Hence, the PMTs should demonstrate a good single electron performance both for the amplitude and the timing response. Furthermore, in order to minimize the probability of random hits during the acquisition, the PMTs should feature a low dark rate.

Another parameter to be kept under control is the probability of the delayed trigger of the system which depends on the PMT after-pulsing rate.

After several tests (see Refs. [26–29]) on the large area tubes available on the market, the 8 in. ETL 9351 phototube, formerly Thorn EMI, was chosen for the Borexino inner detector.

The 9351 tube has a hemispherical photocathode with a curvature radius equal to about 11 cm, resulting in a minimum projected area of 366 cm^2. The cathode coating is made of a layer of CsKSb and the multiplier structure consists of 12 linear focused dynodes (BeCu). The main nominal characteristics of the tubes are summarized in Table 1.

The bulb of the tube is made of a low radioactive Schott 8246 glass that has been carefully studied and characterized underground at Gran Sasso by means of Ge detectors. Results of these measurements are published in [6]. We report here just the main results: ^{238}U:$6.6 \pm 1.9 10^{-8}$ g/g, ^{232}Th:$3.2 \pm 0.3 10^{-8}$ g/g, K_{nat} : $1.6 \pm 0.4 10^{-5}$ g/g.

The ETL 9351 model was chosen taking into account the impact of the main technical features of the candidate tubes on the overall detector performance. For this purpose, the impact of the various PMT parameters and of their characteristics on the final detector performance was analyzed by means of Monte Carlo simulations.

The results of our measurements and simulations, together with the information provided by the manufacturer, were used to define the high priority specification parameters that are shown in Table 2. These specification parameters meet the tight scientific requirements of Borexino and, at the same time, are reasonable enough to avoid a large rejection factor that would have had an unacceptable impact on the total cost of the system.

Table 1
Manufacturer specifications for 8 in. ETL-9351 photomultiplier tubes.

Voltage for gain 10^7	1650 V	Typical
Maximum voltage	2200 V	Max
Maximum cathode-first anode ΔV	900 V	Max
Rise time	$\frac{4}{6}$ ns	Typical
FWHM	$\frac{7}{10}$ ns	Typical
Fall time	$\frac{8}{12}$ ns	Typical
Linearity on peak current (gain 10^6)	8 mA	Typical
Linearity on peak current (gain 10^7)	10 mA	Typical
Linearity on charge (gain 10^6)	$\frac{80}{120}$ pC	Typical
Linearity on charge (gain 10^7)	$\frac{100}{150}$ pC	Typical
SPE peak-to-valley ratio	2.5	Typical
Photocathode sensitivity at 420 nm	26.5%	Typical
Transit time spread fwhm	2.8 ns	Typical
Pre-pulsing ($2\sigma-20\sigma$)	$\frac{3}{6}$%	Max
After-pulsing (0.05–12.4 μs)	2.5	Typical
Dark current at gain 10^7	25 nA	Typical
Dark counts at gain 10^7	3000	Typical

Table 2
High priority parameters and the threshold values used to accept or reject a photomultiplier for Borexino.

High priority parameters	
Photocathode quantum efficiency	>21%
After pulses	<5%
Single p.e. transit time spread	<1.3 ns
Late-pulsing	<4%
Dark count rate	$<2 \times 10^4$ cps
Single p.e. peak-to-valley ratio	>1.5

All listed conditions were required for a photomultiplier to be accepted.

5.1.1. The voltage divider

The main guideline leading the voltage divider design was to maximize the PMT efficiency by shaping the output analog signal. The complete schematic diagram of the voltage divider is shown in Fig. 9. The common linear resistor chain has been chosen, only modifying the resistor values between the first and second dynode, equal to 2 times the common value R, and of that between the second and third dynodes, equal to $1.5R$. As R we chose the value of 1 MΩ, in order to minimize the power dissipation in the divider itself. Signal and HV are coupled/decoupled at the input of the front-end electronics on one side, and at the divider on the other. On the divider side this is accomplished by resistors R2, R3, R4 and C2. The two resistors R2 and R3 have been added to the circuit to optimize the signal shape. The dumping resistors on the last four dynodes (R6, R8, R10, and R12) suppress the ringing associated with the pulse. The 10 nF capacitors in parallel with these resistors keep the voltage constant between the dynodes during the development of the pulse. An "AC-coupled resistor" network (C1/R1, 50 Ω in series with 4.7 nF) has been added to provide some level of cable back termination in order to minimize possible signal reflections on the transmission line. The effect of the capacitor used to ground the 50 Ω resistor is that of adding a negative tail. This compensates, almost perfectly, the positive one, producing a net result of a pulse with a negligible residual tail. The dividers are supplied with

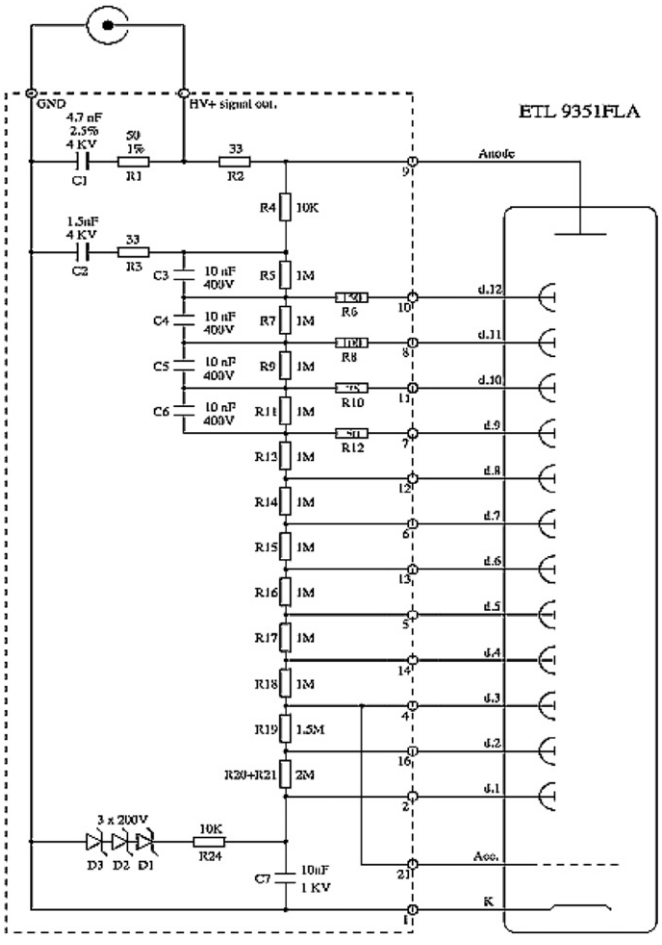

Fig. 9. The photomultiplier voltage divider.

positive high voltage (HV) in the range of 1100–2000 V. The voltage across the cathode and the first dynode is fixed—by means of the Zener diodes D1 to D3—to the value (600 V) suggested by the manufacturer for the optimum PMT performance. A simple R–C low pass filter network (R24/C7) is used here to minimize the wide band noise that might be introduced by the Zeners.

5.1.2. PMT encapsulation, sealing and mounting structure

The 2212 Borexino PMTs are mounted in the detector through equally spaced holes located on the 13.7 m diameter SSS already described in Section 2. The sphere is mounted inside a cylindrical tank and has been filled with scintillator while the tank has been filled with water to act as a final shield against the radioactivity from the surrounding rocks. To assure a reliable operation of the PMTs in such a complex environment, it was necessary to study and develop an encapsulation of the neck of the bulb and the divider. The design has been based upon the broad experience gained in the research and development of the CTF experiment. The base and the neck of the tube are enclosed in a cylindrical stainless steel housing whose external diameter is equal to 90 mm, as shown in Fig. 10. This housing is fixed to the glass of the tube neck through the PC proof EP45HT epoxy resin from Master Bond, which acts as a structural adhesive as well as a protective barrier against PC ingress. The end-cap of the cylindrical housing, welded and helium leak tested (sensitivity 10^{-9} scc/s), carries the feed-through which is inserted into a hole on the sphere surface and then secured through a rear nut. In this way the front part of the PMT is immersed in PC and the rear part in water. Phenolic resin is used as an insulating material that electrically decouples the device to avoid ground loops and also acts as a groove for the viton O-ring assuring the tightness between the tank and the sphere. All 2212 feedthroughs have been tested with a custom made spectrometer, using argon as a trace gas to evaluate the leak rate.

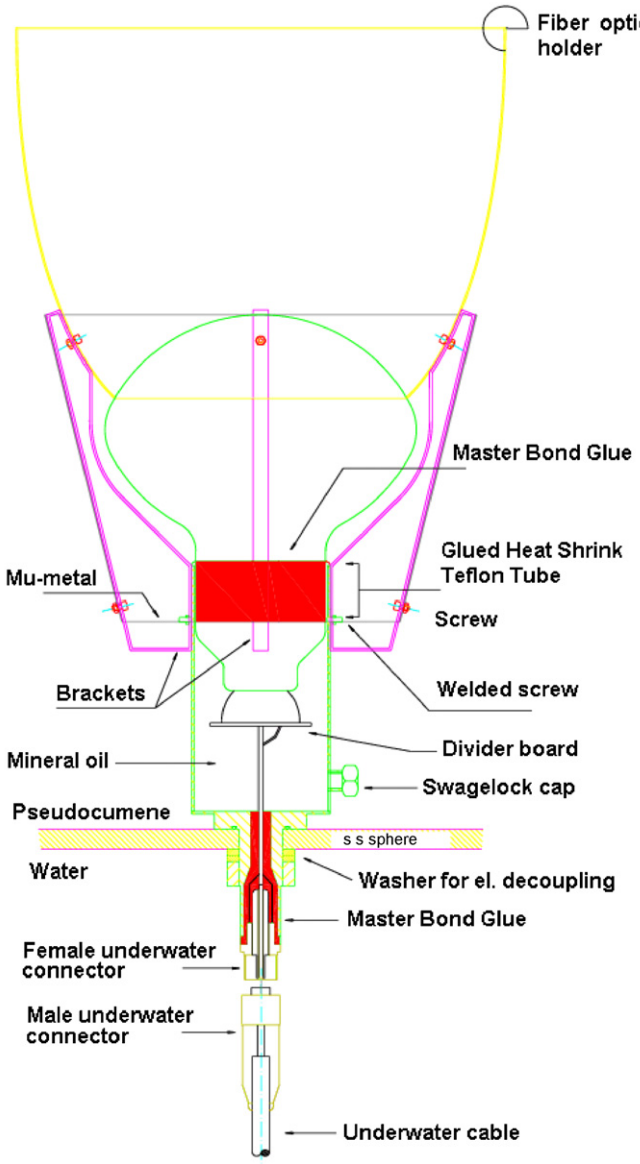

Fig. 10. Design of the Borexino photomultiplier tubes.

It should be reminded that the feed-through is also designed to accommodate the underwater jam-nut connector from the company Framatome. The connector is screwed into the feed-through until its O-ring is properly compressed; a further potting, with the same epoxy resin mentioned before, is also made to have a second barrier against water infiltration. The space inside the cylinder is filled with an inert organic oil inserted inside the can through a 10 mm pipe port sealed afterwards with a Swagelok cap (see Fig. 10). This mineral oil prevents water from condensing on the divider without stressing the very delicate joints between the metal pins and the glass. The last barrier against PC is provided by a heat shrink Teflon tube glued with epoxy resin between the glass neck of the PMT and the steel can. In order to fully benefit from this barrier, we exploited a patented technology of the Gore company which implies a preliminary surface etching of the Teflon film and allows a strong Teflon adhesion on other surfaces.

5.1.3. Optical concentrators and μ-metal

The intrinsic radioactivity of the PMTs used in Borexino does not allow them to be placed close to the center of the detector. In fact, although the PMTs were made from very pure glass, the typical contamination of the glass itself and of the mechanical structure of the PMTs is of the order of 1 Bq/kg, mostly due to Th and K contaminations.

In order to enhance the photon detection efficiency, 1800 PMTs out of the total 2212 have been equipped with optical concentrators (OC). The OC is designed to collect scintillation photons emitted inside the IV with high efficiency and its shape is designed to reflect photons to the curved photocathode of the PMT if the incidence angle is below 32.5°. The OC consists of high purity, soft aluminum which is spinning processed to get its final shape (surface of a body of revolution). The surface was anodized to guarantee chemical stability both in water and in PC. In order to increase specular reflectivity (90% in the wavelength region between 370 and 450 nm) the surface was then manually polished and cleaned. The aging tests confirmed a good resistivity against water corrosion and PC compatibility.

The ETL 9351 PMT, due to its large size, is very sensitive to the Earth's magnetic field. Thus it was necessary to shield it with a conic μ-metal foil (0.5 mm thick) placed around the cathode and the base region. Accelerated aging tests showed that this material, in contact with pseudocumene, strongly catalyzed the scintillator oxidation. It was mandatory to protect the μ-metal with a lining (20 μm thick) of clear phenolic paint from Morton. The support of the μ-metal and the light concentrators is sketched in Fig. 10: it is mounted with four holders at 90°, connected to the housing of the tube with some screws welded onto it.

5.1.4. Cables and connectors

The Borexino cables and connectors will be completely immersed in high purity water for a period of many years. This

has required solutions and materials explicitly developed for submarine applications. The fundamental requirements are material compatibility and electrical performance. Plastics must have a very low water absorption coefficient to withstand long term exposure in water and the design must include multiple barriers against radial and axial diffusion. It is also necessary to avoid effects caused by the concurrent presence of different materials together, such as the development of galvanic couples and of localized corrosion, as well as the release of impurities into the water. Obviously, also the level of radioactivity of the materials is of major concern. The transmission line conducts both the signal and the HV, while assuring the connection to a $50\,\Omega$ front-end where the decoupling of the HV and the signal is accomplished. The cables that connect the PMTs directly to the electronics, are custom made RG 213 coaxial $50\,\Omega$ cables. The outer jacket is made of solid extruded high density polyethylene while a second barrier is made with a laminated copper foil, bound to the braid with a copolymer coating. All cables have an electrical length of 282.1 ± 0.25 ns ($\simeq 57$ m) most of which operates under water. Underwater connectors work in a non-critical condition regarding pressure (the maximum pressure is that of a column of water of 17 m, while these cables are designed for submarine operations), but an immersion time of many years without maintenance requires a very high confidence and experience in long term applications in the submarine field. The company Framatome provided suitably strong stainless steel connectors with viton O-rings. Special attention was also dedicated to the connector cabling to optimize the overall electrical response of the line; dedicated tests with a dual port network analyzer were performed both at the company and at the experiment site.

5.1.5. Design qualification

Various testing stages have been foreseen in order to assess the quality and long-term reliability of the PMT and its encapsulation. As a first step, the device was immersed in its final configuration in deionized water inside a steel tank, to perform an accelerated aging test under pressure and temperature. At the same time, other prototypes were thermally cycled several times in order to identify any possible weakness in the glass-to-metal joint. The results of the tests were compared with a simulation using a finite element analysis. After this first campaign, a more realistic, long term and large scale test set-up was realized at Gran Sasso. A set of 48 PMTs was immersed, at the end of 1999, partially in pseudocumene and partially in water in a two-liquid-tank explicitly designed to reproduce the main geometry, mechanics and environmental conditions of the experiment. The test was successful: after 3 years of testing, all PMTs were working properly and all the main electrical, mechanical and chemical parameters were within the specifications. See Section 12.1 for PMT performance after Borexino filling.

5.1.6. Test system

The PMTs delivered from the supplier (ETL) are factory tested and are provided with the data sheets reporting the operating voltage and other performance parameters. However, due to the difference in the dividers used by ETL and the ones used in Borexino, several of the parameters were measured again. For this purpose a test set-up has been realized at the Gran Sasso Laboratories.

The Borexino PMT test facility is placed in two adjacent rooms. In one room the electronics is mounted, while the other one is a dark room with four wooden tables designed to hold up to 64 PMTs. The tables are separated from each other by black shrouds, which shield the light reflected from the PMTs photocathode. Together with the acceptance tests, the performance of the PMTs while immersed in water was also tested, in order to study the possible mechanical problems for the PMTs to be mounted at the bottom of the Borexino detector. For this purpose, three pressurized WT were installed, each of the tanks can hold up to 20 PMTs. For the purpose of the long-term testing of the PMTs in conditions close to the ones of the Borexino detector a Two-Liquid Test Tank (TLTT) was designed and installed in the laboratory [30]. Forty-eight PMTs are installed in the TLTT, with the base being in water and the bulb immersed in liquid scintillator. The overall test facility is able to measure the characteristics of 172 PMTs if completely loaded. The dark-room is equipped with an Earth's magnetic field compensating system. The non-uniformity of the compensated field in the plane of the tables is no more than 10%. In the WTs and the TLTT the Earth's Magnetic Field is not compensated. All the PMTs under test are illuminated with a picosecond solid state laser (Hamamatsu). The light of this laser is uniformly distributed and attenuated to reach the single p.e. condition. The PMTs are connected through a patch panel to the electronics located in two racks; there are 32 independent channels, quad-multiplexed, to obtain a total of 128 input ports. The system uses the modular CAMAC standard electronics and is connected to a personal computer by the CAEN C111 interface. The majority logic unit LeCroy 4532 is able to memorize the pattern of the hit channels and to activate the reading as soon as one of the signals on the inputs is inside the external GATE on the majority unit. Every laser pulse is followed by an internal trigger used as the majority external gate. One channel of the dark room electronics is shown in Fig. 11. The system performs a preliminary, but very accurate, HV tuning [31] to set the real gain of each PMT at a level of 2×10^7; several parameters are then acquired during a few hour test run and displayed as histograms on the screen in real time. The most important are the charge spectrum, the transit time spread, the after-pulses, and the relative sensitivity (relative quantum and collection efficiency) of the corresponding tube. Using the test facility described above, 2212 phototubes, out of the 2350 delivered by the manufacturer, were selected with the optimal characteristics for Borexino. The precision study of the amplitude and timing response of the ETL 9351 series PMTs has been performed using the test facility, results have been reported in Refs. [32,33].

5.2. The inner detector electronics

The inner detector electronics is organized in 14 identical racks, each of them handling 160 PMTs. Fig. 12 shows a picture of one of these racks. From the bottom to the top, the figure shows the HV mainframes, the digital VME electronics, the front end electronics, the analogue adders and the low voltage power supplies. The following sections describe the main features of these devices.

5.2.1. The HV system

The HV power supply system is based on SYS527 mainframes and A932AP boards, both produced by CAEN[8] s.p.a. (see the bottom of Fig. 12). Each mainframe can house up to 10 boards for a total of 240 channels. However, in order to keep each electronics rack independent from the others and simplify the cable layout in counting room, for the internal detector we have used only seven boards per mainframe, for a total of 168 channels per rack. Only one mainframe has nine boards and it is used to power the PMTs in the WT.

[8] www.caen.it

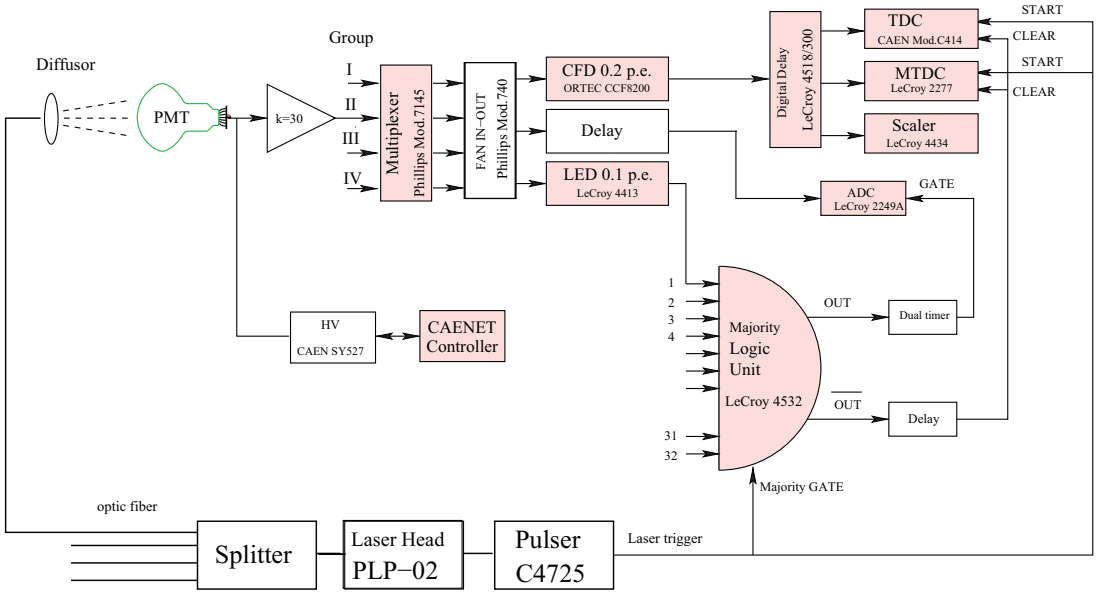

Fig. 11. One channel of the electronics for the PMT test facility.

The A932AP board can provide 24 independent HV channels. The 24 channels share a common HV source, and only the total current drawn by the 24 channels is measured.

The mainframes have a CAENET serial interface that is used to set parameters, control the HV and monitor HV values and currents during data taking. The system is continually monitored by a dedicated slow control server that periodically store the system status into the experiment's data base.

5.2.2. Inner detector front-end electronics

In order to determine the energy and the position of a scintillation event, the amount of emitted light and the time distribution of the p.e. must be measured. For these reasons, the front-end circuit connected to each PMT produces two signals (one for the energy and one for the time measurements) that are processed by the digital boards described in Section 5.2.3.

The number of p.e. collected by the Borexino detector is approximately 500 p.e./MeV and the interesting energy range extends from a few tens of keV up to a few MeV. Therefore, Borexino PMTs work mostly in single p.e. regime, although the probability of having more than one p.e. in a given PMT is not completely negligible, even at relatively low energies.

The signal due to a single p.e. at the front-end input is a pulse having an amplitude of about 12–15 mV and a total width of 15 ns. The multiple hit probability is of the order of 10% for a 1 MeV energy deposit in the detector center. Obviously, this probability increases for off center scintillation events, and at higher energies. The shape of the signal for multiple hit events depends on the scintillation light decay time, the PMT transit time jitter, and the spread of the arrival time of photons on the PMTs. For these reasons, the information about the energy deposit associated with the scintillation event is contained in the total charge collected at the PMTs output within a proper time interval (80–300 ns for single beta or gamma events). Time correlated events, i.e. two isotopes decaying in sequence with the second one having a short lifetime (hundreds of μs or less), are very important for tagging some types of radioactive backgrounds, like U, Th and Rn. The detection of these events with high efficiency requires circuits with dead time in the range of tens of ns or less.

A special analogue gateless charge integrator has been designed to fulfill the energy reconstruction requirements. The circuit works as an ideal integrator always integrating the signal present on the input, without any external gate. The key factor of the integrator design is the AC coupling with the PMT signal due to the presence of a single cable carrying both the HV and the PMT signal. This AC coupling makes the total charge associated with each pulse (single or multiple) equal to zero. The integrator output rises at the pulse arrival time and then decays within a time related to $\tau_{int} = RC$ where C is the capacitor filtering the HV ($C = 4.7$ nF) and R is the 50 Ω cable impedance (for the relatively high frequency PMT signal). This integrator automatically resets itself after each pulse without the use of switches, integration gate signals, baseline restoration networks and it has no dead time. The RC value (500 ns) sets the limit for the maximum frequency of the signals that can be measured. A detailed description of this gateless charge integrator and of the whole front-end circuit is reported in [34].

By sampling the integrator output V at the time t_0 and at the time $t_0 + \Delta t$ ($\Delta t = 80$ ns) the charge Q due to the p.e. arriving within the interval Δt is easily obtained using

$$Q = G(V(t_0 + \Delta t) - V_{off}) - (V(t_0) - V_{off}) \exp^{-\Delta t/\tau_{int}}$$

where $G = 129$ mV/pC is the integrator gain, V_{off} is a DC offset value. The offset value is intentionally added to the output to maintain a positive output polarity in presence of low frequency fluctuations of the output baseline. These are present due to the high gain (close to 10^3 from a few Hz up to about several kHz) of the integrator at low frequency. In this way, the low-frequency fluctuations do not influence the precision of the charge measurement due to the double sampling procedure. High frequency noise components introduce distortions to the integrator output not compensated by this double sampling procedure. The rms value of a fixed charge measurement due to this effect is 3 mV/pC to be compared with the integrator gain of 129 mV/pC.

In addition to the integrator signal, the front-end circuit outputs, for each channel, the PMT signal amplified by two low noise amplifiers with fast transistors. This timing output is fed as an input to a discriminator in the digital board to get the p.e. arrival time. The typical timing signal amplitude is 230 mV corresponding to one p.e. The distribution of the timing output noise level (measured on the 2212 channels) has a mean value of

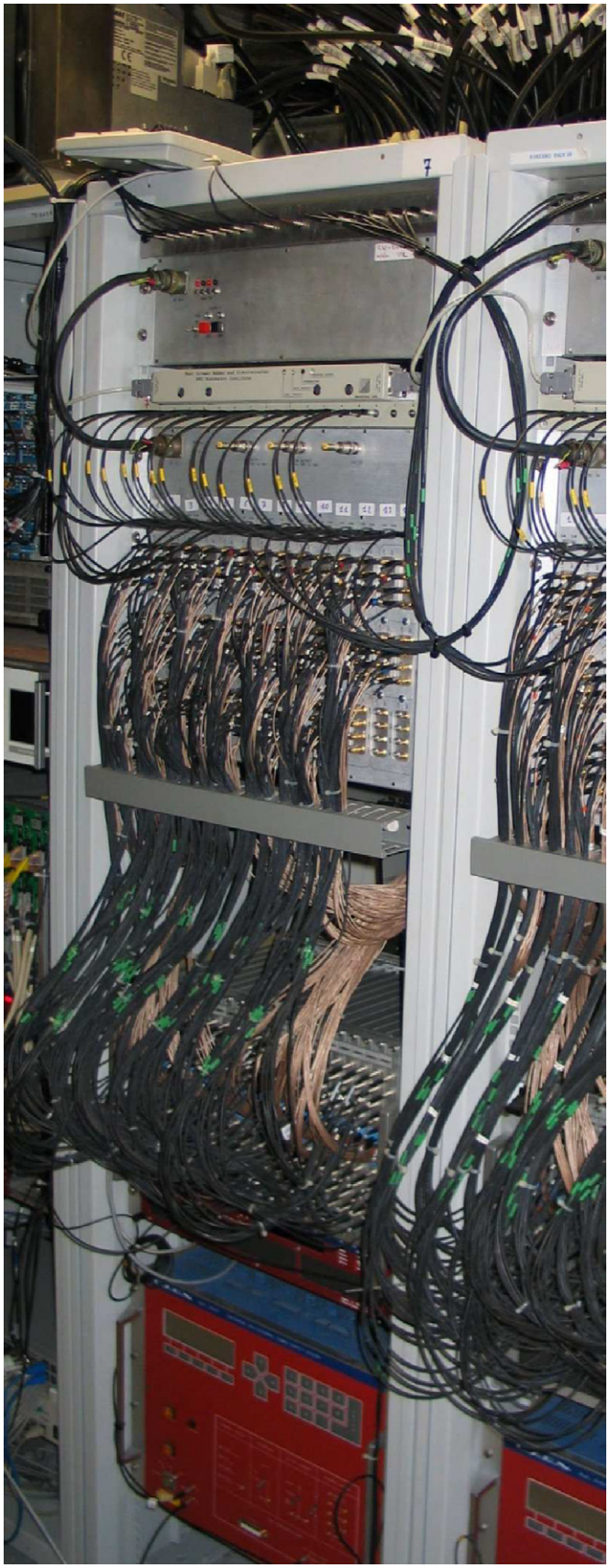

Fig. 12. Picture of the inner detector electronics rack. From the bottom to the top the picture shows the high voltage mainframes, the digital VME electronics, the front end electronics, the analogue adders and the low voltage power supplies.

0.8 mV with 0.4 mV rms with a discriminator threshold corresponding to $\frac{1}{100}$ of the single p.e. amplitude.

The front-end electronics is organized in boards corresponding to high standard rack units. Each board contains 12 single electronics chains and a circuit providing the resistive sum S_{12} of the 12 PMT signals. This sum is used as input to the FADC system described in Section 5.2.4.

The sum chain is linear up to 35 contemporary p.e./channel. Higher numbers of synchronous p.e. lead to saturation of the amplifier that is shared by the sum and the timing circuit. Due to the time spread in the distribution of the number of p.e. belonging to the same event the true sum dynamic range is higher. In addition, a calibration signal can be distributed to all 12 channels.

5.2.3. Inner detector read-out electronics

The inner detector digital electronics provides amplitude and time-to-digital conversion for each front-end channel. Each board houses electronics for eight front-end channels and up to 20 boards can be plugged into a VME crate, for 160 total channels in one electronic rack. Each VME crate is also equipped with a backplane board that acts as an interface to the trigger system. These boards were designed and built in collaboration with Laben s.p.a.

The board architecture is composed of two main functional blocks: the single acquisition channel, replicated eight times and the main control block. The single acquisition channel acquires, asynchronously and continuously, the hits coming from the PMTs. Each channel has two inputs from the front-end stage: an inverted and amplified copy of the fast PMT signal and an integrated output. The fast signal provides the arrival time of the light pulse, while the associated charge (energy) is obtained from the integrated output.

The timing signal is sent to a programmable dual threshold discriminator. The choice of a dual threshold discriminator was done to find the best compromise between a small amplitude *walk effect* and *time jitter* (at the level of a fraction of a nanosecond) and a good rejection of the non-negligible dark rate of PMT pulses smaller than a single p.e.[9] This discriminator is built with two comparators in AND condition: the channel is fired only if the PMT signal crosses the higher threshold but the timing information is related to the lower crossing. The higher threshold is programmable between 0 and 500 mV; a single p.e. signal is about 220 mV and the discriminator threshold currently used in the Borexino runs is about 40 mV, corresponding to about $\frac{1}{5}$ of a p.e. The detection efficiency depends slightly on the PMT pulse shape and is of the order of 95%.

If the discriminator fires, it is automatically disabled for about 140 ns. This dead time was introduced to prevent data jamming during the sampling and the writing of the data on the internal memory buffers. This is a real DAQ dead time only for multiple hits with time delays between 80 and 140 ns. The impact of this dead time on the number of detected hits is of the order of few percent for the typical neutrino events in the fiducial volume. However, whenever two photons hit the same PMT in less than 80 ns, only the timing information of the second one is lost, while the charge sampling is able to keep track of the presence of this second hit.

The discriminator output is used to fire a double pulse generator. Two 30 ns-wide, 80 ns-apart pulses are generated and sent as triggers to a dual input FADC, with 8 bit resolution. The first of the two pulses fires an on-board coincidence unit, that computes the number of activated channels in an adjustable time

[9] The first point would require to set thresholds as low as possible, the second one would instead require higher values.

window of about 50 ns, acting as a first level trigger (see Section 7 for details).

The first FADC channel samples a 10 MHz triangular wave twice.[10] At the same time, the first of the two pulses latches the content of a 16 bit counter (Gray counter) driven at 20 MHz in a buffer register.

The value of the Gray counter plus the knowledge of the ADC sampling of the triangular wave is used to reconstruct the timing information of the hit with a maximum span of 3.2 ms and a resolution better than 500 ps. In order to obtain a good ramp linearity and low noise, special care has been taken in designing the TDC hardware.

The second FADC samples the integrated charge signal. Thanks to a well calibrated delay line, the two samples fall exactly on the baseline and on the peak of the charge pulse.

The ADC and TDC data temporarily stored in an internal memory (local FIFO buffer) are then managed by the main control block, common to all channels of a board. Almost all the functions of this block are executed by a DSP (Digital Signal Processor). The DSP controls the status of the eight channels' FIFO and waits for triggers.

Old data are suppressed by an automatic procedure which every 6.4 μs drops an hit from the FIFO for every channel. A global Daq Gate Signal (DGS) generated by the trigger system and distributed to all boards inhibits this procedure, leading to a programmable read-out time width. Data have been taken with a DGS 7.2 μs wide from May 2007 until December 2007. This value was increased up to 16 μs since then.

When a trigger condition occurs, the Borexino Trigger Board (see Section 7) delivers to the DSPs a master trigger signal, the global gate signal mentioned above, and the 16 bit trigger number identifier. The master trigger signals acts as Common Stop to all the channel FIFOs and interrupts the DSP.

Under this interrupt the DSP starts the procedure to build the data record: all the hits registered in the digital FIFOs are collected and stored in a 8 kbyte Dual Port Ram (DPR), together with a header containing the trigger number. The depth of this memory allows it to store hundreds of typical size Borexino events. The DSP processing time under a trigger condition is 30 μs plus 6.4 μs for each hit. Since the fast coincidences with time delays less than 80 μs are very important for Borexino, the DSP architecture guaranties that the board is able to recover the data of subsequent events occurred during the busy state of the DSP (up to a maximum of 10 events or up to the saturation of the internal FIFOs); this is necessary to acquire the fast coincidences in Borexino.

The DPR is accessible both from the DSP and from a VME bus. A dedicated process running on a VME Power PC computer (PPC) waits for an interrupt to read these data, store them in a single data structure, and send them to the DAQ processes. For more details about the boards and the trigger system see Ref. [35].

5.2.4. The fast waveform digitizer system

The main acquisition system of Borexino has been designed and optimized for the detection of low energy solar neutrinos in the sub-MeV range. A reasonable reconstruction of higher energy events is possible by applying a correction to take into account the saturated channels. However, given the importance of the physics which could be explored by Borexino in the energy range between 3 and 20 MeV (Supernova neutrinos, reactor and Earth anti-neutrinos, etc.), a separate system was designed which is explicitly dedicated to the higher energy range.

This system is based on the idea that at high energies it is possible to retain precision while not having to record each of the 2212 channels individually. The PMT signals are therefore grouped by solid angle sectors, thus reducing the number of acquisition channels. Each of these sums is recorded by a 400 MHz waveform digitizer.

As described in Section 5.2.2, each module of the front-end electronics provides a sum of the fast signals of its 12 channels, obtained by a resistor network. A set of analog adders, active and passive, is used to build, from these sums, 98 groups of up to 24 phototubes, plus the total sum of all channels. These 99 channels are all recorded by fast waveform digitizers.

There are 34 digitizer modules with three input channels each, located in four VME crates, among which 33 account for the 99 analog signals and the last serves to record logical signals such as the trigger. The four VME crates are interconnected by a PVIC[11] bus and read by a single VME master MVME-2302.[12]

The device used was originally designed at APC, Paris, then developed in collaboration with CAEN and produced as *model V896*. It is a VME module housing 3 analog channels, with internal or external clock, a multi-event capability and zero dead time read-out, as long as the read-out occurs faster than the triggering rate. The dynamic range is 8-bits and the sampling period is 2.5 ns.

The V896 is based on a 100 MHz 8-bit flash ADC with a 475 MHz analog bandwidth. Four such flash ADCs, strobed by four 100 MHz clocks, contribute to the digitization of each analog channel. These four clocks, with $\pi/2$ phase shifts are generated internally from a 50 MHz clock.

The waveform digitizers operate in stop mode; they digitize continuously, writing into a circular buffer which we call a page. The storage capacity is 655.36 μs, divided into a configurable number of pages. In Borexino, they are configured as 64 pages of 10.24 μs. On receipt of a trigger they simply leave that page with all the data it contains and start writing to the next page. The written pages can be read anytime by a VME master. This VME master frees the pages it no longer needs, thus allowing the V896 to rewrite them.

The V896 features a 16-bit TTL front panel input that is read when a trigger occurs and is used to associate each page with the event number generated by the main trigger logic.

The 34 V896 modules are synchronized by an external 50 MHz clock; the trigger issued by the main trigger logic is detected and synchronized with this clock by NIM logic and distributed to all the V896 modules. The purpose of synchronizing it with the clock is to guarantee that all waveform digitizers detect the trigger on the same clock edge.

A second level of triggering, equivalent to an energy cut, is performed online by the acquisition process to reduce the amount of data. This second level trigger is done by analyzing the total sum signal. When the amplitude exceeds a programmable threshold, the event is marked to be read, together with other events in coincidence with it, before or after, within a programmable delay.

A further reduction of the data, by a factor of around 20, is performed by keeping only part of the total 10.24 μs time interval of the event: time windows are delimited where the total sum signal exceeds a second programmable threshold. Finally, only the relevant part of the data is read from the VME, formatted, and sent to the event builder. The level of the energy cut is tuned to set the waveform digitizers' data flow to about 50% of the total.

[10] Generated on the board by a triangular wave generator synchronous with the 20 MHz base clock.

[11] The PVIC is a product of Creative Electronics Systems.

[12] The MVME-2302 is a product of Motorola.

The gain of the active adders is adjusted to reach a mean amplitude of 5 flash-ADC counts per p.e. This would lead to a maximum dynamic range of about 50 p.e. if they were all synchronous, leading to a maximum of 12.5 MeV at the center of the detector and much less at the limit of the fiducial volume. Actually, due to the dispersion in the emission time of the photons, the simulation shows that, for the whole fiducial volume, the mean value of the energy loss due to saturation reaches about 1% at 10 MeV. Since saturation occurs, by definition, with high amplitude signals and high amplitude signals are not subject to large statistical fluctuations of their shape, the lost energy is recoverable by fitting the expected pulse shape on the unsaturated part of the signal.

6. The OD

Even though the rock shielding reduces the muon flux by a factor 10^6, high energy muons originating within cosmic ray interactions in the atmosphere are still able to penetrate to the depth of the Gran Sasso laboratory. In this context they constitute a relevant source of background for the experiment and must be tagged with high efficiency for the success of the ^{7}Be neutrino flux measurement as well as of the rest of the physics program.

Among the tagging methods, a key role is played by the OD, a water Cherenkov detector composed of 208 additional PMTs installed in the volume of the WT, where an ultra-clean water buffer is present for shielding purposes.

The PMTs are of the same model of those used for the inner detector (8 in. encapsulated ETL 9351) and are arranged on the outer side of the SSS and on the floor of the WT. The PMTs parameters are summarized in Table 1. The PMTs must work in water and under almost 2 atm of pressure at the WT bottom. Therefore, their mechanical arrangement, the connectors and the cables are designed and chosen to be reliable in these conditions.

Unlike those mounted inside the sphere, OD PMTs are equipped with a full encapsulation (see Fig. 13). This is a stainless steel cone-shaped case, housing the PMT, the voltage divider, the μ-metal shielding and a female HV connector. The μ-metal shielding is a thin metal foil required to protect the PMT against the Earth's magnetic field that could spoil the time resolution. The HV connectors mate with 55 m submarine cables identical to those used for inner detector PMTs. These cables carry both HV and the signal connecting the PMT to the electronics chain. The sensitive photocathode is covered only by a transparent PET foil (the transparency is 90–92% in the frequency range of interest), so the PMT retains an acceptance angle close to 180°. The space between the case (including the PET foil on the front) and the PMT is filled with mineral oil in order to minimize the index of refraction discontinuities in the light path to the photocathode. A detailed description of the encapsulation design and its pressure tests can be found in Ref. [36].

In order to increase the light detection efficiency, most of the WT and SSS surfaces (≈ 95%) are covered with sheets of Tyvek, a white paper-like material, ∼200 μm thick, made of pressed polyethylene fibers.

In the original detector's layout the 208 PMTs were arranged in 12 horizontal rings on the outer SSS surface, every PMT looking radially outward. In this way the 590 m^2 surface of the SSS was populated with one PMT every 2.8 m^2 (1.7 m linear average distance) and, according to simulations, the 99% detection efficiency required to suppress the muon flux was met.

However, though not strictly required for the ^{7}Be primary physics goal of Borexino, the additional possibility of reconstructing also the track of the through-going muon is of fundamental

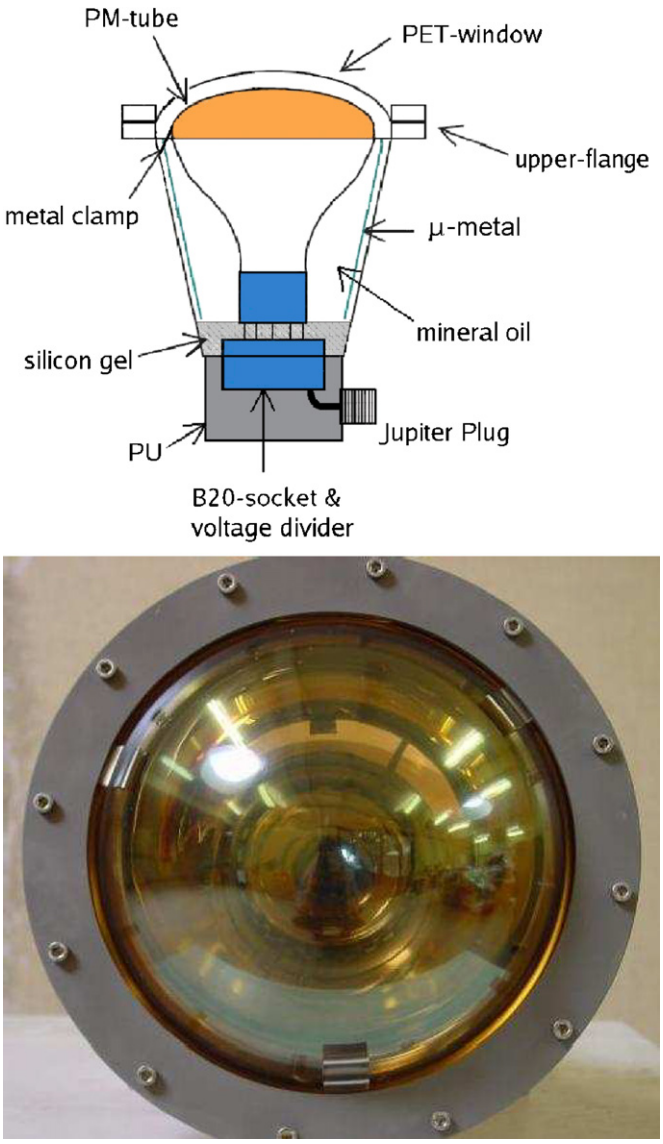

Fig. 13. Sketch of the encapsulation of the outer detector PMTs (top) and a front picture of an encapsulated PMT (bottom).

help in the reduction of ^{11}C background for *pep* and CNO measurements. This ambitious goal requires the highest possible efficiency of direct light detection, reflected light being of hinderance in this respect. In the new design, the lowest quarter of the PMTs are re-positioned on the WT floor looking upward in five concentric rings. This is a structural feature of the WT: along the circular perimeter of the floor, the volume up to a height of ∼1.5 m and degrading inward for about the same length is filled with massive steel for engineering reasons. This offers a comfortable surface with a ∼45° inclination where installed PMTs look roughly toward the sphere. Monte Carlo simulations have shown that this configuration reduces the amount of reflected light detected by the PMTs, without spoiling the muon detection efficiency.

As said earlier, each PMT is connected to the electronics via a single cable that brings both HV and the signal. Unlike the ID electronic chain, the HV decoupling is not performed within the front-end electronics, but is performed externally in custom decoupling boxes (HVDs) with a high pass filter circuit. The signal goes from the HVD boxes to the front-end electronics.

The front-end electronics of the OD is made of 14 Charge-to-Time Converters (QTCs).

The board is a 9U single VME unit which takes only power from the VME backplane with no connection to the data-way bus. One QTC board is made of 16 channels.

Each QTC converts the analog signal coming from the PMT into a differential digital signal whose time duration (distance between the trailing and the leading edges) is proportional to the total charge of the pulse. The output of the QTC is connected to a commercial double-edge TDC (CAEN v673). The TDC measures the time of the two signal edges with respect to the common stop provided by the trigger system. The first rising edge yields the time of the PMT pulse, while the time distance to the second falling edge yields the charge.

Besides this main function, each QTC provides two additional signals that are used for triggering purposes, the so-called secondary and tertiary outputs. The secondary output is a one-per-board analog step function pulse whose height, in steps, represents the number of channels firing in coincidence. Both height and width of the steps can be adjusted. The width defines the coincidence window. All secondary outputs (14, one per QTC board) are sent to the Muon Trigger Board (MTB) for the Outer Muon Trigger (OMT) formation. The Tertiary Output (TO) is a one-per-board analog pulse given by the sum of the input signals with a built-in fixed amplification factor of about 2. These outputs are sent to an additional analog trigger formation system.

7. The trigger system

The main requirement for the Borexino triggering system is to be able to identify, quickly and efficiently, scintillation events that are detected by the quasi-simultaneous occurrence of several PMT hits. Due to the large number of PMTs, and the relatively high total dark current, we designed a triggering system using purely digital logic.

The trigger should fire when a programmable number of PMTs (typically a few tens, see below) are hit within a short trigger time window (TTW). The TTW must be set to be larger than the maximum arrival time spread of photons at the PMTs. Being the total transit time of photons throughout the SSS at most about 50 ns, the system allow the TTW to be set from a minimum of 48 ns up to a maximum value of 99 ns. The typical value used during data taking was 60 ns (see Section 13). The energy threshold is set by the 156 keV ^{14}C β decay end-point energy. Although this background cannot be removed, it is very important to collect at least the last part of the ^{14}C β spectrum for calibration and monitoring purposes. With a nominal effective yield of about 500 p.e./MeV, this requirement brings the triggering threshold down to about 40 photons.

In order not to miss the double coincidences from fast radioactive chains, and particularly the ^{214}Bi–^{214}Po coincidence of the ^{238}U chain whose mean decay time is 236 μs, the system must have a short recovery time. Therefore, the whole system is implemented using combinatorial logic (implemented in a set of Field Programmable Gate Arrays, FPGAs) and a DSP that supervises and controls the logic. The DSP and all FPGAs are housed in a custom made VME board that is controlled and read by a dedicated Power PC of the same type used for data taking.

The system works as follows: as described in Section 5.2.3, each digital crate is equipped with a backplane board that is capable of counting the number of hits occurring within a TTW. Particularly, every 16–33 ns (one period of the common 30–60 MHz programmable clock that is distributed throughout the system) each digital crate counts the number of channels in which the PMT signal exceeds the analog threshold.[13] At each clock edge, this number is the total number of counts that have occurred in the previous three clock cycles, making the 48–99 ns TTW range stated above. This 8-bit number is synchronously sent to a set of Trigger Adder Board (TAB) via a flat cable with differential Positive ECL (PECL) signals every 16–33 ns. There are five TAB boards in the system. Four of them perform the sum of a group of four crates (there are 14 crates) and the fifth one perform the sum of the output of the other four TABs. At the end of this chain, every 16–33 ns the output of the fifth TAB yields the total number of hits detected in the previous 48–99 ns. This number feeds the input of the Borexino Trigger Board (BTB), a custom made VME readable board that implements all triggering logic by means of programmable FPGAs and a Texas Instruments TMS320C50 DSP. When the total number of hits exceeds the programmed threshold, the DSP is interrupted, and the trigger sequence begins: the triggering signals are generated, the absolute time is read from a GPS clock and a trigger record is written in the VME readable memory. In this way each event is labeled with its unique 16 bits event number and its absolute time is known with about 100 ns accuracy.

The BTB handles several additional triggers, besides the main one described above: every 0.5 s, a random trigger, an electronic pulse trigger and a timing laser trigger are fired for monitoring purposes. In a random trigger, an event is read regardless of the detector status; in an electronics pulse trigger, a pulse from a pulse generator is sent to the test input of each front-end channel; in the timing laser trigger, the laser system and the OD Light Emitting Diodes (LEDs) described in Section 9 are fired. For the purpose of sub-ns time alignment, the signal sent to the laser and LEDs systems is also copied and sent to a set of spare data acquisition channels. By means of these three triggers we can identify the number of valid channels in each run and disentangle the reasons for failure. This is of particular relevance for Borexino, because the stability of the energy calibration is a crucial feature for observing the seasonal variation of the neutrino flux.

A special triggering mode was introduced a few months after the beginning of data taking to cope with the necessity to acquire the spallation neutrons produced by muons crossing the scintillator. In fact, we have observed from the data that ≈ 70 times per day a muon produces one or more spallation neutrons that propagate in the scintillator and are finally captured by a proton with the emission of the characteristic 2.26 MeV gamma line. The capture time is about 250 μs. For several analyses (^{11}C cosmogenic background tagging, anti-neutrino and others) it is very important to detect these neutrons efficiently (see also Fig. 38 in Section 13.4). The original triggering scheme used from May 2007 until the end of 2007 did not allow this because of an intrinsic dead time present in case of three or more consecutive triggers in a time window of 1 ms. To solve this problem we have modified the logic so that every time a muon (identified by the OD) crosses the SSS, a very long gate of 1.6 ms is issued instead of the standard gate. In this way all neutrons can be acquired.

A triggering system is also required for the outer muon detector. As described in Section 6, the QTC boards are capable of providing an analogue signal whose height in steps is proportional to the number of channels that fired in coincidence. These QTC secondary signals are sent to a custom VME board, the MTB, which allows us to set a threshold on the number of PMTs

[13] This threshold is set to $\frac{1}{5}$ of the p.e. signal amplitude. After front-end amplification, the single p.e. signal amplitude is about 230 mV; the threshold we set is 40 mV.

firing in coincidence, and sends a signal to the BTB. When the MTB signal arrives, the BTB initiates the normal trigger sequence that is used for any other trigger. The typical threshold used for physics corresponds to about 6 PMTs.

The whole detector, both internal and external, is always read-out for any trigger type. For more details about trigger logic see Refs. [16,37].

8. Data acquisition system

All the inner detector digital boards have a VME interface and are organized in crates hosting 20 boards and a VME Single Board Computer (SBC). The OD TDCs and the Flash ADC boards are also VME based and are read by means of the same kind of SBC (one crate for the OD readout and four crates for the Flash ADCs). The data are read crate by crate by the SBC and sent through the network to a workstation. The VME computers (Motorola MVME 230×) are based on the Power PC (603e) CPU and on the Universe VME/PCI bridge; the operating system running on these machines is Debian GNU/Linux with the 2.2.12 kernel. The performance of the system in a real-time analysis has been studied; the interrupt latency has been found to always be lower than 100 μs, with a mean of 20 μs. The SBC are diskless and a cross-development setup has been installed on the i386 based workstations. See Ref. [38] for details.

The read-out is trigger based: once the system is started, the trigger signal is propagated to all the racks where the SBCs collect the data from the digital boards for network delivery; as soon as all event fragments are received by the builder workstation, the full event is reconstructed and written to disk. At the end of the run all the data are sent to a Raid storage, in a compressed form (the compression algorithm and a MD5 hash, assure that the data cannot be modified).

The data throughput is dominated by ^{14}C, the largest source of trigger rate; a concentration of about 3×10^{-18} g/g corresponds to 250 Bq of β decay in the active volume. Depending on the threshold, the trigger rate can be up to 100 cps with a mean energy of 150 keV; this produces a data flux of the order of 50 kbyte/s and a total storage of about 4 GB per day. These numbers are compatible with a simple network design, based on 100 Mb/s ethernet technology with a switched layout. A full private network setup has been installed (with private IP addressing compatible with RFC1597) and router/firewall interconnects the Gran Sasso LAN with the Borexino one; the system includes all the facilities commonly found in a full network deployment.

The data acquisition system is controlled by a set of web pages which in turn interact with the different processes using CORBA. A PostgreSQL database is used to maintain the run information (like the start time, the disabled channels list and so on), which are necessary for the analysis and calibrations. The entire code has been developed in C, C++ and in Perl scripts.

The maximum data flux that the internal read-out can sustain is a 400 cps trigger rate with high energy events (one hit per channel which is approximately equivalent to the deposit of a 5 MeV β-particle); this high rate fulfills all the Borexino physics goals. The main use of such a high trigger rate is for laser calibrations.

9. The PMT calibration system

Borexino relies on the precise determination of the time of flight of the photons from the location of the scintillation event in order to reconstruct the event position and to define the Fiducial Volume. Furthermore, the knowledge of the total charge collected by each PMT is important for the energy determination of high energy events. For these reasons, both time and charge calibration of the PMT system is of utmost importance. Therefore, a multiplexed system of optical fibers has been developed for the precise PMT calibration both in time and in gain.

Precision in the time measurement of single hits affects directly the position reconstruction precision. Position resolution is limited by the scintillator fluorescence decay time of 3.5 ns (effectively increased to 5.5 ns after light propagation effects [14]), by the PMT transit-time jitter of ~1 ns and by the inter-PMT time equalization, which should be maintained at the sub-nanosecond level and is regularly checked. The precision of the time measurement is also crucial for α/β discrimination, based on the different fluorescence time profiles for α and β scintillation events (see Ref. [39]). An accurate energy determination and resolution are crucial for the spectral shape recognition of the neutrino signal: the energy resolution of the detector depends on good charge calibration, the energy being determined, through a proportionality relation, from the number of detected photons or from the total charge collected by all PMTs.

9.1. System design

In the design of the calibration system for the time and charge response of the Borexino PMTs the following requirements have been taken into account:

(i) accuracy in time equalization: inter-photo-multipliers equalization inaccuracy should be lower than the PMT time jitter, which is ~1 ns;
(ii) accuracy in charge calibration: the system must illuminate all 2212 PMTs at the single p.e. level in order to measure the Single Electron Response (SER) parameters of each PMT. If we require less than 1% contamination from multi-electron pulses and from the dark noise accidental coincidences, the illumination level should be, respectively, lower than a mean value $\mu = 0.05$ p.e. and higher than $\mu = 0.01$ p.e. [30];
(iii) linearity check: the PMT illumination level should be adjustable, in order to verify the linearity of the PMT response. The value of ~8.6 p.e. corresponds to the saturation limit of the front-end electronics (in an 80 ns interval): higher intensity calibration sources would allow non-linearity studies;
(iv) calibration rate: the PMT calibration should be performed at the fastest rate allowed by the DAQ system (a few hundreds Hz at an illumination level of $\mu = 0.05$ p.e.), in order to minimize the duration of the measurement;
(v) operational convenience: the system should allow a high level of automation for frequent use and must be operable from outside (a remotely controllable system also meets the requirement for a synchronization with the main electronics);
(vi) radioactivity: the contamination induced by the calibration system materials must not add a significant rate to the dominant (unavoidable) background generated by the PMTs;
(vii) long-term reliability, for at least 10 years of data taking.

Several alternative solutions were considered that could suit the detector geometry consisting of consecutive shielding regions. The simplest method would be a light diffuser in the center of the detector (as in the SNO experiment [40]), illuminating all the PMTs simultaneously. However, a permanent diffuser would not be acceptable since it would represent a constant source of radioactivity in the innermost region, while a removable one

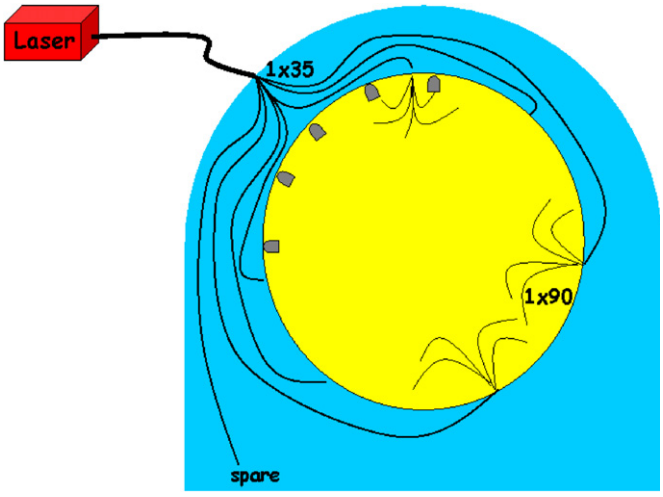

Fig. 14. Scheme of the multiplexed laser system for photomultiplier calibration. A single very short laser pulse is distributed to all PMTs through a set of optical multiplexers and fibers.

would not allow for the simplicity and safety of operation needed for frequent calibrations. Permanent light diffusers could be placed in the buffer region (as in the LSND [41] experiment), or light beams could be generated by optical fiber couplers in the SSS; in both of these solutions, the light would cross several meters of the buffer and scintillator regions, requiring off-line corrections to the light-pulse arrival time: the consequent dependence on the scintillator properties (such as index of refraction and attenuation length), which could drift in time, would compromise the calibration accuracy.

The solution adopted for Borexino is based on a different idea: the light emitted by an external laser source is carried simultaneously to each PMT tube by a dedicated system of optical fibers. As shown in Fig. 14, the laser light is first distributed to 35 fibers which reach the SSS in 35 different points. Light enters the SSS via 35 custom designed optical feedthroughs and is again split into 90 fibers each individually coupled to a PMT. In this way, radioactive contamination is avoided since no part of the system is immersed in the innermost part of the detector. Furthermore, light reaches the photocathodes without crossing a large amount of scintillator and/or buffer liquid, thus avoiding dependency on the medium characteristics. The entire fiber system design follows a requirement of mechanical decoupling of the internal/external regions to facilitate the mounting operations:

- air/water interface: a fast light pulse emitted by an external laser is focused onto a bundle of 35 external fibers 40 m long, running in the water buffer region;
- water/SSS interface: the 35 external fibers reach different locations on the sphere supporting the PMTs. Each single external fiber couples to a proper optical feed-through on the SSS itself;
- SSS/PC buffer interface: each feed-through is coupled to a bundle of 90 internal fibers 6 m long, running inside the SSS and reaching every single PMT.

9.2. PMT calibration light source

The light source is a diode laser (*PicoQuant* LDH400), emitting a fast (50 ps time width) light pulse at a wavelength of 394 nm, where the photocathode quantum efficiency is about 27%. The maximum peak power is 400 mW, corresponding to 1.7×10^7 photons/pulse. The laser driver (PDL 800-B) allows a maximum repetition rate of 40 MHz, well above the maximum rate of the Borexino DAQ system and can be triggered by an external pulse to allow synchronization with both main electronics and DAQ; laser intensity can be selected by means of a potentiometer which, by design, is only manually adjustable (an upgrade of the controller allowing remote setting of the intensity is under study).

The optical components associated with the coupling of the laser to the first segment of the calibration system consists of a series of neutral density filters for attenuation and a lens to focus the beam on the surface of a 2.5 mm diameter rigid quartz fiber (cladrod) that then distributes the light to the 35 fiber bundle. The lens is a 10× standard microscope lens; focusing is necessary since the area of the laser spot (2×3.5 mm), is larger than the quartz fiber core. The rigid quartz fiber is 10 cm long and its numerical aperture is lower than the 35 fiber bundle area, for better optical transmission. The optical apparatus is mounted on a passive anti-vibration platform and enclosed in a light-proof stainless steel box; the laser controller can be activated from outside the box.

9.3. External fibers

As previously said, the laser beam illuminates the fiber bundle of the first splitting point through a focusing lens and an optical rod that renders it uniform and wide enough to cover 35 quartz fibers. The diameters of the fiber core and cladding are 300 and 325 μm respectively. The fibers enter the detector through a single feed-through on the top of the WT and form separate cables, with Kevlar strands (for mechanical resistance) and a polyethylene coating, until they reach their entry points on the SSS. The PMTs are grouped in 28 clusters of about 80 elements. For mounting reasons, the tubes installed on the 3 m main entrance door require an extra fiber bundle. The locations on the SSS are chosen as the central position of each PMT cluster. Six out of the 35 fibers are spare.

9.4. Light-transmitting feed-through

A delicate part of the system is the feed-through on the SSS, since it must distribute the light from 1 input to 90 output fibers as uniformly as possible, while maintaining a high level of tightness against liquid transfer between both sides of the SSS. The body and the connectors are made of electro-polished stainless steel, the sealing with the stainless steel flange is accomplished with a Viton O-ring. A quartz fiber, of length 10 cm and diameter 1.5 mm, is placed inside the connectors, optically coupling the PC and the water buffer side. The sealing against PC diffusion by capillarity near the fiber is assured by filling the inner part of the feed-through with a PC-proof, quartz-steel adherent epoxy resin.

9.5. Internal fibers

The second step of the multiplexed chain is formed by coupling the SSS feed-through to a bundle of 90 quartz fibers of 110 μm core diameter (Fig. 15). Taking into account the packing ratio of circles on a plane, 90 closely packed fibers with a diameter of 120 μm (cladding) occupy an area of 1.12 mm^2. The cross-sectioned area of the 1.5 mm diameter fiber in the feed-through is 1.76 mm^2, thus a tolerance of 50% for non-optimal packing of the fiber bundle is achieved.

Both internal and external fibers, as well as the lens and clad rod used at the beginning of the optical path, have a quartz core, in order to optimize light transmission efficiency in the ultraviolet wavelength region. The cladding of the external fibers can be

Fig. 15. A bundle of 90 fibers connected to the feed-through and illuminated.

Fig. 16. A picture of an installed photomultiplier: it shows the optical fiber used for timing and charge calibration and the Teflon support attached to the light concentrator.

made of plastic, while the strong chemical reactivity of pseudo-cumene determines the choice of quartz for the cladding of the internal fibers. This is one of the reasons for using Teflon for the coating of the internal cable; in addition, measurements carried out by the collaboration showed that Teflon has a very low rate of Radon emanation. A Teflon support attached to the PMT light concentrator points the fiber termination in the direction of the photocathode, at a 20 cm distance (Fig. 16).

9.6. System feasibility tests

During the design phase, several tests were performed to guarantee the feasibility of the system for Borexino. On the one hand, the compliance of the system with the general requirements of the experiment in terms of radioactivity and chemical compatibility had to be verified and on the other, the total light transmission expected at the end of the chain had to be measured. The attenuation due to geometrical effects and fiber transmission can indeed be safely gauged from the a priori known fiber characteristics, while the inefficiency caused by losses at optical couplings can only be measured in the final experimental conditions. The results of the system feasibility tests are described in detail in Ref. [30], along with the light transmission properties measured on the assembled and installed system.

9.7. OD calibration system

The main goal of the OD is to tag muons crossing Borexino in order to exclude them from the samples of events used for the neutrino analysis. Moreover, since muons can produce radioactive spallation products inside the scintillation core, it would be important to reconstruct the muon track in order to spatially correlate it with a subsequent internal event. In order to develop refined muon tagging tools and to perform a reliable muon track reconstruction it is important to know precisely the relative arrival times of each Cherenkov photon at the phototubes. However, the transit time of a signal through a PMT tube and the electronics to which it is connected can differ from one channel to another by several nanoseconds. It is therefore mandatory to develop a calibration system to perform the time alignment of all channels within 1 ns by means of a light pulse sent simultaneously to all PMTs. The idea is similar to the one

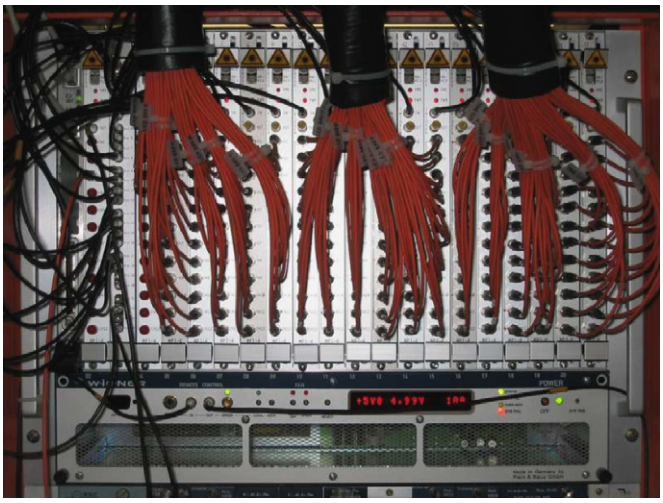

Fig. 17. The outer detector calibration system. LEDs housed in electronic boards deliver light pulses to PMTs in the Water Tank through individual optical fibers (orange).

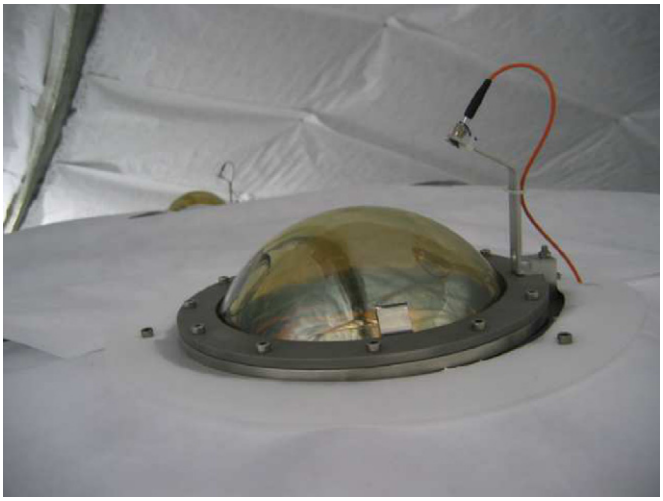

Fig. 18. The outer detector calibration system: the tube enclosing the fiber and its mechanical support are visible above the PMT glass.

described in the section for the inner detector. The OD PMTs are operated in a wider dynamics than the ID ones: even though it is difficult to quote an average hit occupancy for a muon event since this strongly depends on the geometry of the track, simulations show that PMTs can easily detect bursts of 50 or even 100 p.e. if directly hit by the Cherenkov cone. On the other hand, PMTs seeing only light diffusively reflected by the Tyvek surfaces will yield very few p.e. Although the PMT linearity is not in question, a reliable calibration should extend as much as possible in the operational dynamic range. It was therefore decided to develop a calibration system for the OD capable of working both in single p.e. mode, as well as in charge regimes up to 40 p.e. (and possibly beyond). The system is made of 208 LEDs, each one delivering the light pulse to one PMT in the WT through an optical fiber. The optical fiber is mounted on the PMT with a steel support that holds it about 8 cm and 30° off-axis. Considering the opening angle of the fiber (15° semi-aperture) the support was designed for 100% geometrical efficiency and minimal shadowing of the photocathode. Figs. 17 and 18 show the layout of the system.

10. Optical calibration of the scintillator and buffer liquid

As already mentioned, the energy and position reconstruction in Borexino rely critically on the optical properties of the scintillator and buffer liquid. The number of emitted photons and their time distribution depend on the scintillator; the number of detected photons and their arrival time depend on the transparency of the media they cross. Many studies have been performed in the laboratory to measure critical parameters of the scintillator and buffer liquids, such as the emission and absorption spectra, interaction length and so on. Unfortunately, the extrapolation of these results to a large–volume 4π detector like Borexino may not be straightforward (see for example the CTF data [14]) and it is therefore necessary to check them *in situ*. Furthermore, since Borexino will take data for many years, it is important to keep the relevant optical parameters of buffer and scintillator under control during the experiment's lifetime, in order to make sure that no significant variations occur. For example, it is known that some mixtures of organic scintillators can change their light absorption properties when exposed to a large amount of untreated steel for an extended duration of time [42].

For these reasons, we have implemented a system which allows a non-invasive and easy monitoring of the optical properties of the detector liquids by sending laser light of different frequencies through different portions of the detector. A schematic view of the system is depicted in Fig. 19. It consists mainly of three parts:

(i) Lasers. In order to probe the optical properties of the detector at different wavelengths, two lasers are available: one is the diode laser already described in Section 9.2 ($\lambda = 394$ nm). The second one is a solid state laser which emits light at $\lambda = 355$ nm.
(ii) Optical fibers. The laser light is carried inside the detector by means of 31 single fibers which enter the SSS in 31 different positions. The system is designed to work with only one fiber at a time, in order to collect data with the light coming from a single point on the sphere: the selection of the fiber is performed via an external patch-panel.
(iii) Feed-throughs on the SSS. They are of two types: the *radial type* and the *oblique type* (see Fig. 19). There are 11 *radial* feed-throughs and they are designed to shoot light radially through the detector. In order to collimate the light beam, they are equipped with a small lens and a pin-hole aperture. The *oblique* feed-throughs are designed to shoot light at an angle such that it crosses the buffer liquid only and not the active scintillator. In order to do so, the feed-throughs are equipped with a pointing device (Fig. 20) which aims precisely at a selected target PMT. The target PMTs have been chosen at different distances from the feed-throughs in

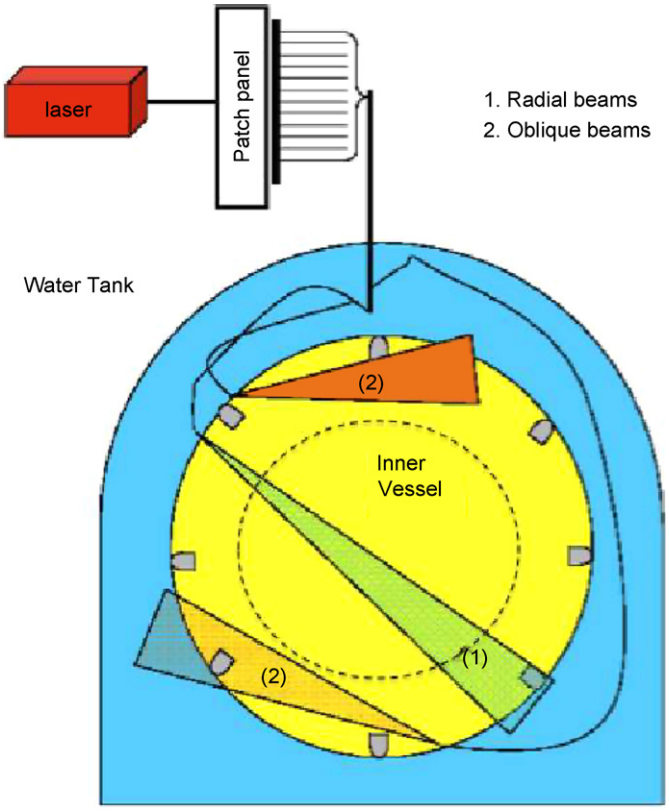

Fig. 19. Scheme of the system to monitor detector transparency: the laser light is transmitted by means of optical fibers through the Water Tank into the SSS. The picture sketches the light beam in case of *radial feed-through* (1) and *oblique feedthroughs* (2).

Fig. 20. The pointing device for the *oblique* type of feed-through: the photo shows a module already installed on the Borexino Stainless Steel Sphere and surrounded by PMTs. The device is designed to point laser light at an angle towards a specific target phototube. The angle is chosen so that the light crosses only the buffer liquid and not the active scintillator.

order to probe attenuation of light after different path lengths: depending on the feed-through, the distance which the light crosses before reaching the target PMT ranges from a minimum of 2.5 m to a maximum of 7.88 m.

The monitoring strategy dictates that we perform, periodically ($\sim$ once per month) some dedicated runs shooting laser light both through the buffer liquid using the *oblique* feed-throughs and through the buffer + scintillator using the *radial* feed-throughs described above. In this way, it is possible to study the transparency of the two media while undergoing both absorption and elastic scattering processes: we recall that absorption reduces the total amount of collected light (and therefore affects energy reconstruction), while scattering changes the time distribution of detected photons thus affecting the position reconstruction and α/β discrimination capability. The laser light at $\lambda = 394$ nm can be used both for *radial* and *oblique* beams since in this wavelength region scattering on pseudocumene is the dominant process (with an interaction length of approximately $\sim$5 m). The laser light at $\lambda = 355$ nm can be only used to study the buffer transparency and not the scintillator one since the absorption and re-emission process on PPO at this wavelength would completely block light crossing the scintillator. At this wavelength the expected scattering length of PC is $\sim$2.5 m. Thanks to the fact that both the radial and the oblique beams are collimated (depending on the type of feed-through, the opening angles range between 2° and 6°), it is possible to measure the scattered and transmitted light separately thus performing a periodic monitoring of the detector's optical response. Collecting data with *oblique* beams with target PMTs at different distances also allow measurement of the absolute PC attenuation length. In order to have redundancy of information and to keep the systematics under control, the *oblique* system has more than one beam crossing the same distance. For more details about this monitoring and calibration system see Refs. [43,49].

11. Internal source calibration system

11.1. Motivation

In order to complete the scientific program, and particularly to measure the solar neutrino fluxes, the Borexino detector must be carefully calibrated.

As shown by several studies done with Monte Carlo simulations, and confirmed by our first measurement of ^{7}Be neutrinos [2], the main sources of uncertainty in the measurement of the solar neutrino fluxes are:

(i) The knowledge of the fiducial mass, i.e. the inner most part of the scintillator that is used as the neutrino target and whose volume is defined by means of a cut on the reconstructed position of the events. An accuracy of ± 2 cm is required for the knowledge of the radius of the fiducial volume.
(ii) The knowledge of the energy scale for α, β, and γ particles.
(iii) The knowledge of the detector energy response as a function of the event position within the fiducial volume, of the particle type and of the energy itself (non-linear effects).

Additionally, the optimization of the α/β separation, and a precise knowledge of its efficiency, as a function of particle energy is crucial for several physics analyses.

It is worth noting that some of these problems can be addressed by studying some internal radioactive contaminants in the scintillator. However, the bulk activity is generally not sufficient to study the detector response well enough.

For these reasons, we have developed a system for the insertion of radioactive and light sources in the Borexino bulk. This system must fulfill stringent requirements in terms of radiopurity, cleanliness, mechanical strength and reliability, and must guarantee complete air tightness while inserting, operating, and removing the sources from the detector.

With the use of this system, a suitable set of α, β and γ sources can be put into various accurately known positions within, and at the border of, the fiducial volume, so that the complete detector response can be determined.

11.2. Cleanliness requirements

The chief concern of an extensive calibration campaign must be the minimization of the risk of detector contamination. The system described in Section 11.3 was designed to insert, position, locate, and remove a radioactive or fiber optic calibration source in a manner that does not pose undue risk to the vessels or contamination of the scintillator. All components that come into contact with IV scintillator have been electropolished, pickled and/or passivated with proper acids, washed with suitable detergents, rinsed with ultra-pure water until particulate counting reached class level[14] 20. This class level 20 corresponds to a contamination of about 2×10^{-16} g/g when the contaminant is present in the dust at the ppm level, the typical value for LNGS dust both in Thorium and in Uranium.

The most critical components are housed inside of a glove box under a Low Argon and Krypton Nitrogen (LAKN) atmosphere [44] in order to prevent accumulation of Radon and other isotopes on their surfaces when not in use. In addition to the strict cleaning procedures, redundancies in critical instrumentation, and a very detailed operational procedure have been implemented in order to reduce the risks of contamination to a suitable level.

11.3. Description of the system

The system can be effectively broken down into two subsystems—insertion and location. The insertion system provides a means to place a source at any location inside the IV, while the latter is used to provide feedback on the precise location (± 2 cm) of the source. A brief description of each follows.

11.3.1. Insertion system

The insertion system was designed to insert three devices into the detector: radioactive calibration sources, fiber optic calibration sources, and a scintillator sampling tube that can be used for detector monitoring purposes. The radioactive sources are small quartz spheres (radius 2.5 cm) containing the desired isotopes as well as a small volume of scintillator, whereas the fiber optic sources are cylindrical quartz vials which contain the fiber optic terminations and also the LED used for location.

The sources are attached to the end of a series of neutrally buoyant stainless steel rods, 1 m in length, with an optional hinged section which allows the assembly to be rotated up to 90°. The rotation of the hinge is accomplished by pulling on a Teflon tether tube attached to the source coupler. The entire assembly can also be rotated azimuthally 180° in either direction to map out cylinders in the IV.

The insertion operations are performed through a custom built glove box (see Fig. 21) which resides in a class 10 clean room atop the Borexino WT. Located between the glove box and the IV fill tube is a load lock where the sources are attached to a spring

[14] MIL-STD 1246C.

Fig. 21. The glove box used for source insertion. Some of the insertion rods are visible at the left of the glove box.

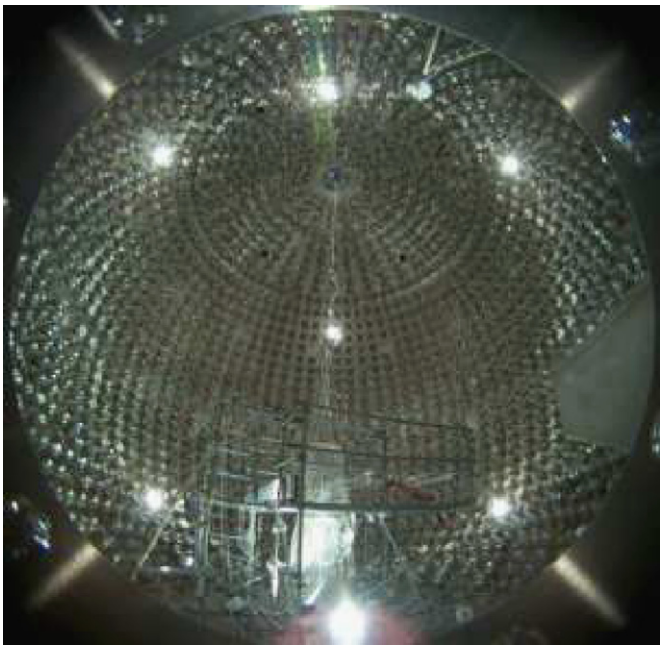

Fig. 22. The sphere during the nylon vessels installation. The picture also shows the position of six out of the seven cameras (the bright spots). The 7th is of course the one that took the picture.

loaded rod coupler. The insertion rods and Teflon tether tube pass through sliding seals since there is a significant pressure difference between the glove box and the load lock. The glovebox, load lock, and the sliding rod seal, are continuously purged with LAKN during operations to avoid introducing any radioactive contaminants into Borexino during a calibration operation.

All of the instrumentation for the insertion system is computer controlled and monitored, with several interlocks and alarms to

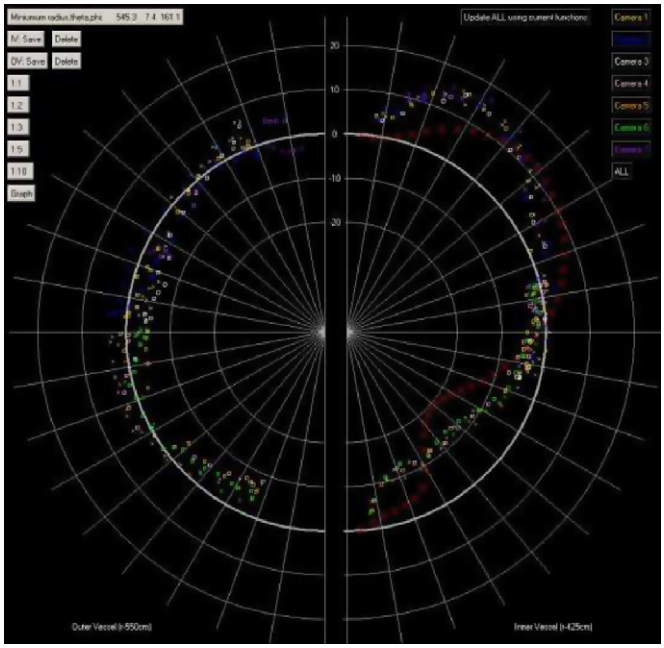

Fig. 23. This image shows the deviation in cm of the radius of the nylon vessels for each of the seven cameras. Each color refers to a different camera (see Fig. 22). The white line is the Inner Vessel nominal position projected in the plane orthogonal to each camera. The points show the reconstructed position in the same plane. The maximum deviation from the ideal spherical shape is less than 20 cm in radius (each white circle in the figure corresponds to 10 cm deviation from ideal shape).

alert operators before any damage is caused to Borexino. Once the source has been inserted and positioned into the predetermined site, the location system (described below) goes to work.

11.3.2. Location system

The system described above does not provide enough feedback to determine the position of the source to the level of precision required. Thus it was decided to equip every source with a light source, and use a system of seven digital cameras to find the position of the source. The cameras used are consumer grade Kodak DC290 digital cameras, each of which is equipped with a Nikon FC-E8 fish eye lens. During 2002, this system was tested with a string of LEDs suspended in the center of Borexino and the ability to locate the sources to within 2 cm was verified (see Ref. [45] for details).

The camera system has also proved to be a valuable tool for vessel monitoring, particularly during inflation and filling operations; all pictures of the internal part of the SSS that are shown in this publication and elsewhere are taken with this system. A software package was written to present the collaboration with many analysis tools for deconvolving the images taken during the water and scintillator filling processes. Fig. 22 shows the position of six out of seven cameras, the 7th being the one that took the picture.

The camera pictures can be analyzed with an associated image processing software. This software reconstructs the position of the nylon vessels with an accuracy of a few cm. Fig. 23 shows the reconstructed position of the IV as viewed by the different cameras and its deviation from the nominal shape.

12. Detector performance

A preliminary study of the performance of the Borexino detector has been carried out during several test runs (the so-called *Air runs*)

before the detector was filled. These runs, which occurred between 2002 and 2005, offered a unique opportunity to debug and tune-up the whole detector. During these runs it was possible to check the PMT tube status and the full read-out chain performance. It was also possible to make a complete test of the online and DAQ system. The trigger system was finalized and the possible trigger configurations (see Section 7) were defined. Several dedicated runs with the laser were made, in order to develop and validate the timing and charge calibration procedure.

12.1. PMT failure rate

All 2212 PMTs except for a few tens located on the floor of the SSS were installed in Borexino in the years 2001–2002. The remaining PMTs were installed in 2004 right after the installation on the nylon vessels and immediately before closing the SSS. Because of the well known problems at the Gran Sasso Laboratory, in the years 2002–2006, the PMTs remained in air, being only occasionally operated in a few air runs. During this time, about 50 PMTs were lost, most of them showing flashing problem, i.e. the emission of light from the bulb due to vacuum loss.

The filling of the SSS with ultra-pure water began on August 2006 and finished in November 2006. During this period about 80 PMTs were lost, most likely because of defects or cracks in the sealing. We observed a clear infancy effect, i.e. the failure rate was much higher at the beginning, and most PMTs died shortly after having been submerged by water.

During the beginning of January 2007, until May 2007, the water in the SSS has been replaced by PC and, at the same time, the WT was also filled with ultra-pure water. Even in this case, we observed a high failure rate for a few weeks, mostly because of imperfect or damaged connectors or cables in the WT (we recall here that the PMT connectors pass through the SSS and are immersed in the water of the WT).

The total number of dead PMTs at the beginning of data taking was 175. Since then, the failure rate has gone down significantly, reaching the current plateau of about 3 lost PMTs per month. At the time of writing (May 2008) the number of dead PMTs is 206 out of 2212.

12.2. Charge and time calibration

As discussed in Section 9, the precise determination of photon arrival time at the PMTs is crucial for Borexino to perform an accurate position reconstruction of the events and for pulse shape discrimination purposes. Also, the measurement of total collected charge is used to determine the energy of the events. For these reasons, an accurate and periodic time and charge calibration of the PMTs is of utmost importance. To accomplish this, a multiplexed optical fiber system has been designed which was described in detail in Section 9. The calibration strategy adopted for Borexino [46] requires that dedicated runs are taken periodically (at least once per week) with the laser on. During these runs a NIM timing unit simultaneously delivers a driving signal to the laser and a trigger signal to the main Borexino electronics. A copy of this signal is also sent to dedicated electronics channels to precisely measure the time delay between the laser pulse and the arrival time of photons at the PMTs. The laser is usually driven at a repetition rate of 100 Hz. The light intensity is selected in order to work at the single p.e. level on each phototube. In these conditions the statistics for a good calibration run can be collected in less than 1 h. The typical plot of the time difference between the laser trigger and the response of the phototubes to the laser light is shown in Fig. 24 (summing several thousands events and including all PMTs): the plot shows

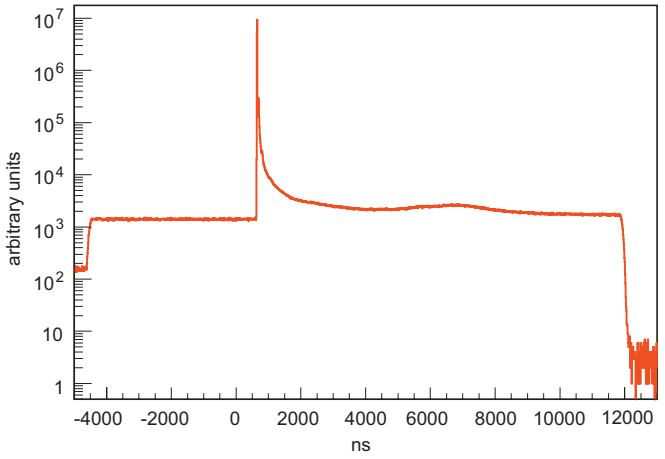

Fig. 24. Time response of all photomultipliers to the laser pulse in a typical laser run before any time alignment: the laser peak is clearly visible on a plateau of uncorrelated random noise hits. The data acquisition gate of about 16.5 μs is also visible. Although the intrinsic laser pulse is very narrow in time, the peak has a width of several tens of ns (with tails up to hundreds of ns) because of the light reflection and propagation on the PMT glass and on the SSS surface. Note the vertical log scale.

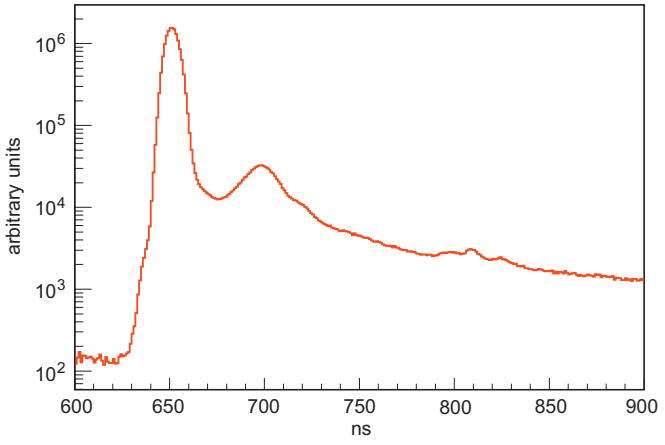

Fig. 25. This figure is the zoom of Fig. 24 between 600 and 900 ns within the gate. The main laser peak is clearly shown, together with two additional peaks that are due to reflection of light on the glass and its propagation through the SSS. The diameter of the SSS is 13 m and the refractive index of PC is 1.5. The position of the second peak is in good agreement with the expected maximum value of 64 ns.

the 16.5 μs acquisition gate where the laser signal is clearly visible on top of a much smaller plateau of hits due to uncorrelated dark noise of the PMTs.[15] In Fig. 25 (a zoom of Fig. 24) the time spread of the laser peak is visible. The second peak about 60 ns after the first one is due the light that is detected on the other side of the SSS after being reflected by the PMT glass.

The width of the laser peak is an indication of the time spread of the PMT response before any time alignment, since the laser light is sent simultaneously to all phototubes with an accuracy much better than 1 ns. The sigma of the distribution is approximately 4 ns before alignment. In order to reduce this spread, the time response is studied individually for each PMT and the position of the laser peak is calculated via a Gaussian fit; the computed calibration constants are then written in the Borexino database and are used during the data processing to

[15] In 2007 the acquisition gate was 7.2 μs and has been changed since January 2008 in order to reduce the dead time.

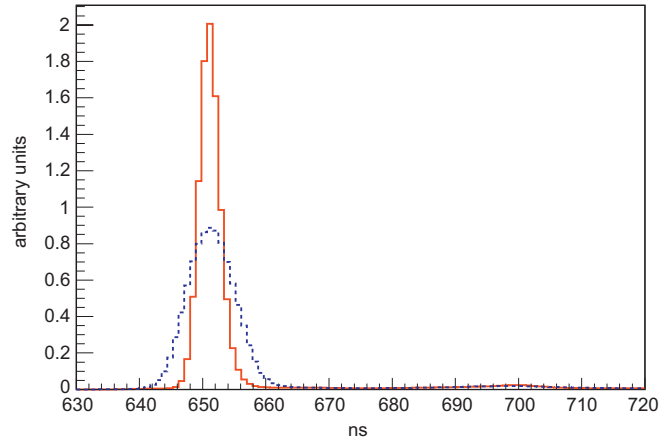

Fig. 26. Time response of the phototubes to the laser pulse before time alignment (blue dotted curve) and after time alignment (solid red curve). The width of the peak is reduced to the expected value of 1.6 ns. The wide shallow peak around 700 ns is due to the reflection of light on the PMT glass. This light is then detected on the other side of the SSS.

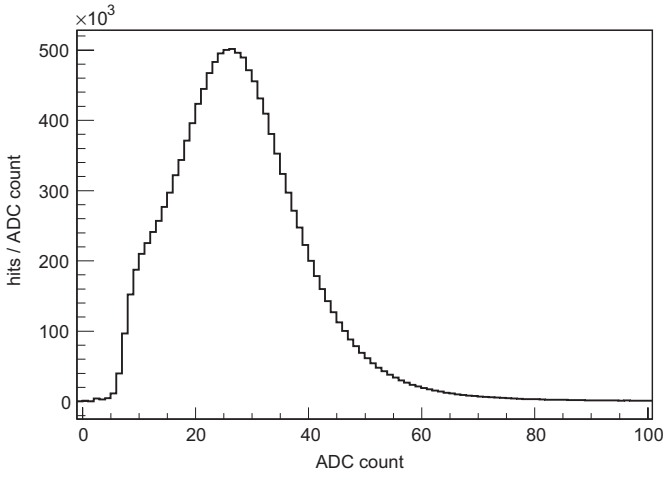

Fig. 27. Charge response of the phototubes (in ADC units) for a typical laser run. The distribution is the sum of all live PMTs (about 2050). One photoelectron is approximately 25 ADC counts.

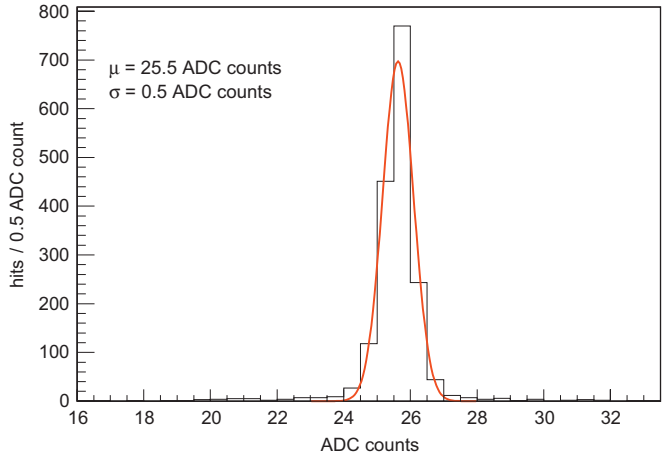

Fig. 28. Distribution of the position of the single photoelectron peak for about 2000 PMTs. The position is computed by fitting the single photoelectron peak using laser events. This uniformity was achieved by choosing the PMT high voltage appropriately. No software correction is applied to the charge gain.

correct the response of each phototube on a channel-by-channel basis. Fig. 26 shows the response to the laser light for all phototubes before and after time alignment: the width of the Gaussian is reduced by the calibration procedure to 1.6 ns, an excellent result which is consistent with the unavoidable residual effects of PMT time jitter and intrinsic time resolution of the electronics.

The same laser pulses are used to monitor the charge response of each phototube. Fig. 27 shows the charge spectrum (in p.e. units) for all phototubes after calibration. The gain of all PMTs have been equalized by choosing the optimal value of their HV. Fig. 28 demonstrates that we managed to adjust the gain to be uniform within a sigma of less than 1 ADC count.

13. Data analysis

In January 2007, Borexino began filling with scintillator. A few weeks later, the detector was turned on and the first data were collected. Data taking continued during most of the filling and allowed detector monitoring and final hardware and software tuning, and shifter training. Borexino filling was completed on May 15th, 2007. The first available data have been very useful to understand the overall performance of the detector, in terms of energy and position reconstruction, the capability to tag delayed coincidence events, the capability to disentangle α and β particles, and the muon tagging efficiency. In the following, we report a few analysis results whose only purpose is to show that the hardware described in this paper is working as expected. The following is neither comprehensive nor should be regarded as a list of final results. A future paper will report the details of the analysis techniques and the final detector performance.

13.1. Scintillation events

An event in Borexino is a collection of PMT hits occurring within a time window of a few tens of ns with a long tail that can reach a few hundreds ns. When the trigger fires, however, all hits occurring within the DGS of 16 μs are recorded (see Section 5.2.3 for details). In this long gate both the signal hits and the random noise hits of the 2212 PMTs are recorded. Although the number of random noise hits is relatively small (about 1 μs to be compared with a signal of about 100 hits in less than 200 ns at 200 keV), a software procedure is necessary to identify both the beginning of the scintillation pulse and its end. We define a *cluster* a collection of hits belonging to the same scintillation event, and we

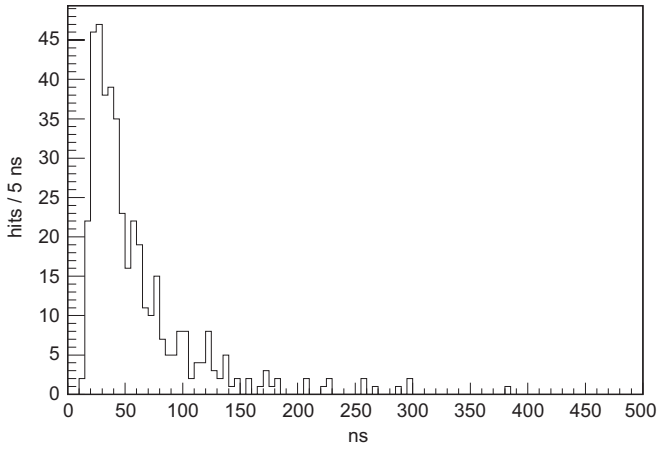

Fig. 29. Time distribution of the PMT hits in a single cluster event.

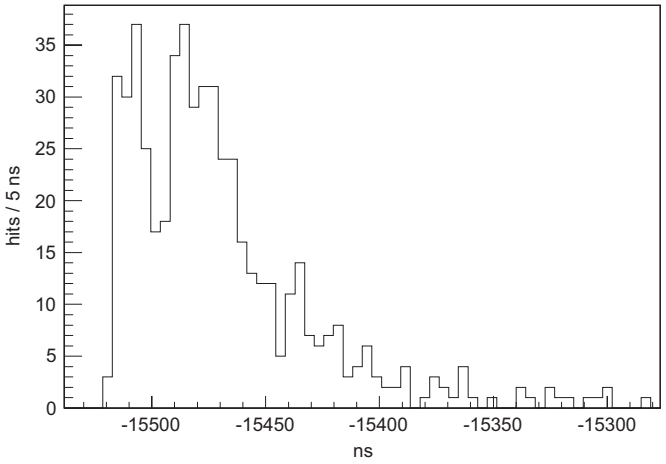

Fig. 30. Two clusters partially overlapped and identified by the splitting software. The time distance of the two clusters is in this case about 25 ns. Clusters as close as 15 ns can be efficiently identified.

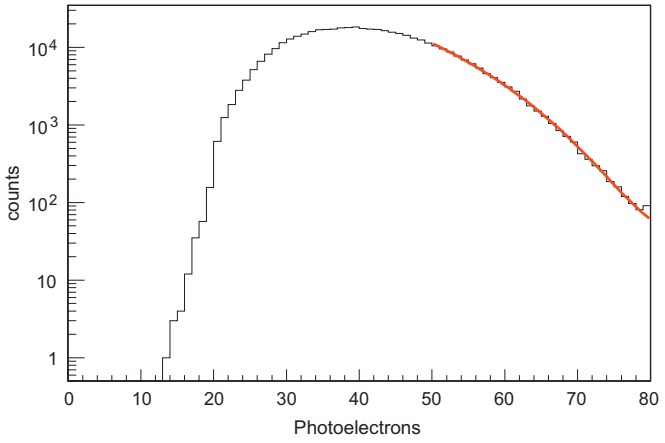

Fig. 31. Low energy portion of the Borexino spectrum: a fit is performed to the ^{14}C beta spectrum including the effect of beta ionization quenching, the beta decay form factors and the background shape. The spectrum does not start from 0 photoelectrons because of the trigger threshold.

call *clustering* the offline software procedure that is applied to identify the *cluster*. A typical cluster is shown in Fig. 29.

The *clustering* procedure determines the time position of the rising edge of each *cluster* with a resolution of less than 1 ns, allowing the measurement of the time difference between close events with that precision.

Each *cluster* is also analyzed to check whether it is compatible with being a unique scintillation event or it is the overlap of more than one event. This is important both to reject pile-up events and to identify very fast coincidences like those due to ^{212}Bi–^{212}Po decay or ^{85}Kr. Fig. 30 show an example of a two cluster event, a good ^{212}Bi–^{212}Po candidate.

The time distribution of the hits within the cluster allows the reconstruction of the position of the event, the determination of the total energy deposited in the scintillator and the discrimination of α and β particles. The following sections describe these points in more detail.

13.2. Energy and position reconstruction

One of the most crucial points for Borexino is the energy resolution, which ultimately depends on the light yield, i.e. number of p.e. per MeV collected by the PMTs. A preliminary measurement of the detector light yield was obtained by fitting the shape of the ^{14}C spectrum: we recall that the ^{14}C isotope is present in an organic liquid like pseudocumene and is therefore an unavoidable background which affects the low energy part of the Borexino spectrum (β decay with an endpoint of 156 keV). Fig. 31 shows the beta spectrum of ^{14}C and the result of the fit: the fitting function includes the effect of energy resolution, beta ionization quenching (through the Birks' factor K_B, see for example Ref. [47]), the beta decay form factors and background parameterization (exponential + one Gaussian). The resulting conversion factor, normalized to 2000 phototubes, is found to be approximately 500 p.e./MeV. The systematic error associated with the fit is estimated to be of the order of 5%.

The presence of some radon caused by a small air leak (a few liters) which developed in the system during filling afforded the opportunity to further understand the performance of the detector: we recall that ^{214}Bi and ^{214}Po are two isotopes produced in sequence in the radon chain. ^{214}Bi decays by beta or beta + gammas (Q value = 3.23 MeV) emission, while ^{214}Po decays via alpha emission ($E_\alpha = 7.7$ MeV). The short lifetime of ^{214}Po ($\tau = 236.6\,\mu s$) gives the opportunity to tag the two event sequence

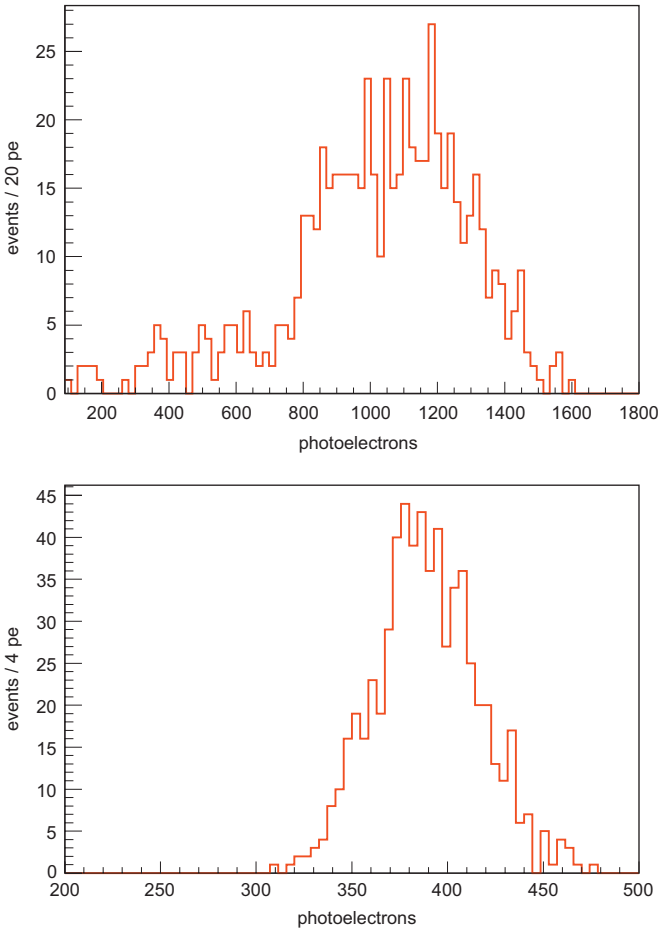

Fig. 32. Energy spectrum for the first (top) and second (bottom) event which pass the coincidence selection cuts. The first plot is compatible with the expected $\beta + \gamma$ spectrum of ^{214}Bi. The second plot clearly shows the ^{214}Po alpha peak. The events are all selected in the fiducial volume (100 ton nominal) and correspond to about 1 year of data. The relatively poor statistics is a consequence of the extreme purity of the scintillator.

very efficiently providing a sample virtually free of background. Fig. 32 shows the energy of ^{214}Bi and ^{214}Po candidates after requiring that the two events have occurred within a time window smaller than 5 times the ^{214}Po lifetime. The first plot is

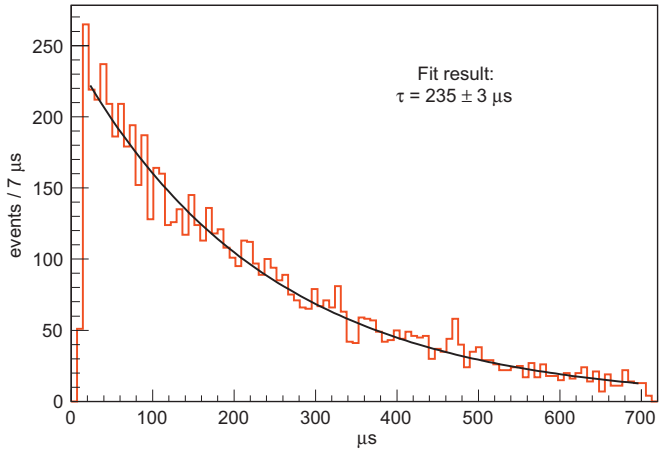

Fig. 33. Time difference between the first and second event of the ^{214}Bi–^{214}Po coincidence sample (see text for selection cut details). A fit with an exponential + a constant is performed. The resulting lifetime is $\tau = 235 \pm 3\,\mu s$.

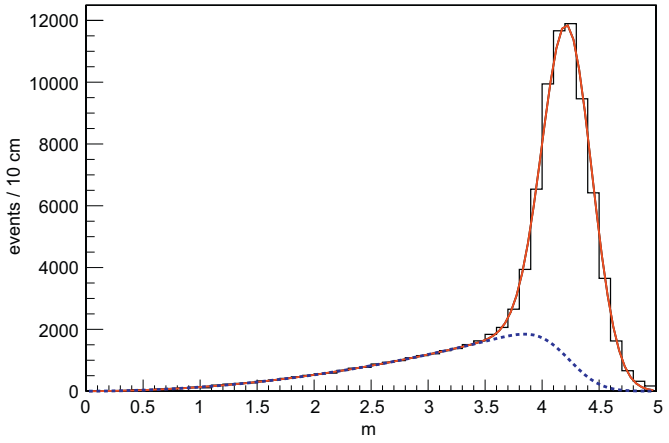

Fig. 35. Reconstructed radius for events in the energy region between 100 and 200 photoelectrons. The distribution can be fit with two contributions: the internal one (blue dotted line) and the external one (red continuous line).

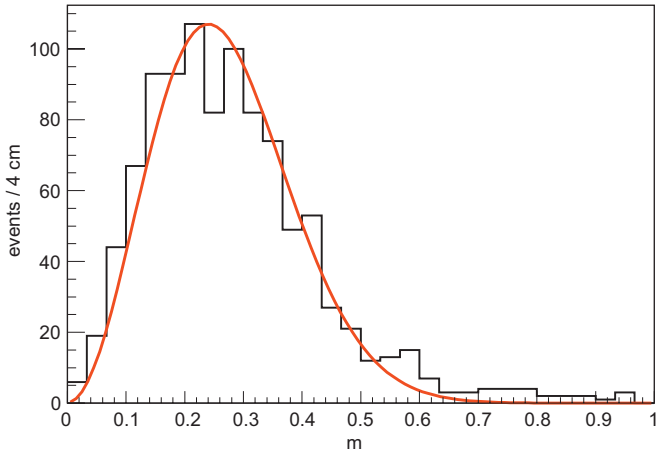

Fig. 34. Distribution of the distance between the two events of a ^{214}Bi–^{214}Po coincidence. From this plot, a resolution of 16 cm is obtained by fitting the distribution with the correct expected curve (not a Gaussian).

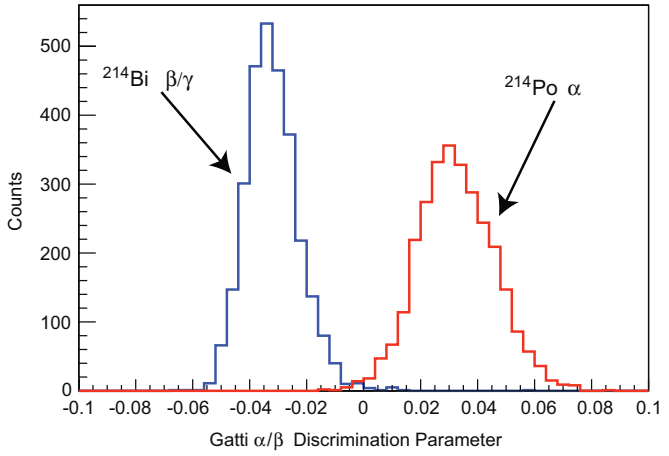

Fig. 36. Gatti variable for ^{214}Bi–^{214}Po events. The two components are clearly separated.

compatible with the $\beta + \gamma$ spectrum of ^{214}Bi, while the second plot clearly shows the ^{214}Po alpha peak. The reconstructed energy resolution is 7% (1σ). It is worthwhile to notice that the position of this peak corresponds to an equivalent energy on the beta scale which is approximately $\frac{1}{10}$th of the nominal alpha energy; this reduction of light in the case of alpha particles is due to the well-known light quenching effect [47]. Selecting only events under the ^{214}Po peak and plotting the time difference between the first and second event, one obtains Fig. 33: a fit to the time difference with an exponential plus a constant (to account for the background of random coincidences mostly coming from ^{14}C events) gives $\tau = (235 \pm 3)\,\mu s$ which is in very good agreement with the expected ^{214}Po lifetime. The sample of ^{214}Bi–^{214}Po coincidences also provides a useful tool to study the performance of spatial reconstruction algorithms. Since the ^{214}Po lifetime is very short compared to the typical diffusion time, the two events occur exactly in the same position. Therefore the reconstructeddistance between the two events depends only on the spatial resolution of the reconstruction algorithm.[16]

[16] Some care should be taken because ^{214}Bi decays 81% of the time emitting a γ, and therefore the light barycenter could move from the decay position.

Fig. 34 shows the histogram of reconstructed distance for the clean sample of coincidence events. By fitting the distribution with the correct non-Gaussian distribution, the position resolution at these energies is found to be 16 cm, in good agreement with expectations and Monte Carlo simulations.

The position reconstruction is the crucial tool to define the fiducial volume by means of a software cut. As an example, Fig. 35 shows the radial distribution of events detected in the energy region between 100 and 200 p.e. The plot can be fit as the sum of two contributions: the internal volumetric distribution (mainly due, in this case, to ^{210}Po alphas) which goes as r^2 and the external background distribution (mainly due to PMTs radioactivity) which is well approximated by a Gaussian centered at the vessel border.

13.3. α–β *discrimination*

The ^{214}Bi–^{214}Po delayed coincidences provide a nice and clean sample of α and β events that can be used to develop and tune the α/β discrimination algorithms. We recall that these algorithms are based on the different time response of the scintillator to α and β particles (see Fig. 8). In this paper we just show the results of the effectiveness of α/β separation based on the Gatti optimal filter [48]. Fig. 36 shows the Gatti variable for the α and β samples obtained from the ^{214}Bi–^{214}Po analysis: the two curves are very

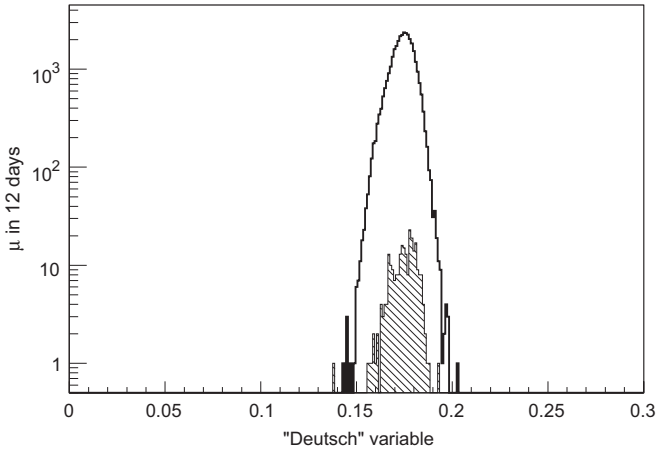

Fig. 37. Outer detector muon tag efficiency. The full curve is the distribution of muon events selected by means of the inner detector requiring at least 6000 photoelectrons collected by the PMTs. The shaded area is the distribution of muons that do not have an outer detector tag. From the figure, an efficiency of $>99\%$ is measured. The x-axis variable ("Deutsch" variable) is the ratio of the collected charge seen by inner PMTs without light cone divided by the total inner detector charge.

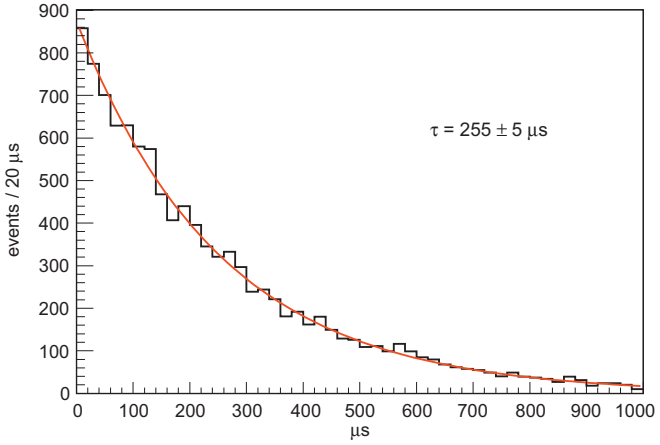

Fig. 38. Distribution of the spallation neutron capture time in the scintillator. Muons crossing the scintillator or the buffer occasionally produce spallation neutrons that are then captured by protons and detected by means of the emitted gamma from deuteron.

well separated. It should be pointed out that the α/β discrimination power is expected (and verified) to be energy dependent and to get worse at lower energy. A comprehensive study on this issue will be reported in a future paper.

13.4. Muons and neutrons

Finally, we have performed a preliminary study of the muon tagging efficiency. Both inner and outer detector can identify muons. The OD does so by means of the Cherenkov light produced in the external WT by the crossing muons. A study of the detector behavior shows that, with a threshold of 6 p.e., the muons are very efficiently detected with negligible random noise. The inner detector can separate muon events from scintillation events by means of several shape variables. In this paper we do not discuss this matter further, except to show the OD efficiency measured by means of a clean sample of muons that cross the inner detector. This sample is selected requiring a huge energy deposit in the scintillator (>6000 p.e.). Fig. 37 shows that the efficiency of the OD for this class of events is $>99\%$. In the physics analysis, the muon rejection is done using both outer and inner detector capabilities. The detailed study of the overall muon tagging efficiency will be reported in a future paper.

We can also efficiently detect spallation neutrons produced by the muons crossing the scintillator volume. The neutrons are quickly thermalized in the scintillator and are captured by protons with the emission of the characteristic 2.26 MeV gamma. Fig. 38 shows that the capture time distribution is in good agreement with the expected value. This result was obtained after the modification to the triggering scheme described in Section 7.

14. Conclusions

The construction and the commissioning of the Borexino detector is completed. Data taking has begun on May 15th, 2007 and is going to continue for several years. This paper shows that the detector meets, or in some cases exceeds, the expected performance. The radioactive background is lower than the design values for several contaminants, particularly for the ^{238}U and ^{232}Th daughters. The PMTs of both inner and OD, the electronics, and the trigger system work as expected.

Acknowledgments

We sincerely thank the funding agencies: INFN (Italy), NSF (USA), BMBF, DFG and MPG (Germany), Rosnauka (Russia), MNiSW (Poland), and we acknowledge the generous support of the Laboratori Nazionali del Gran Sasso. This work was also supported by the ILIAS integrating activity (Contract no. RII3-CT-2004-506222) as part of the EU FP6 program.

This paper is dedicated to the memory of Cristina Arpesella, Martin Deutsch, Burkhard Freudiger, Andrei Martemianov and Sandro Vitale, and to John Bahcall, a friend and strong supporter of Borexino.

References

[1] G. Alimonti, et al.Borexino Collaboration, Astropart. Phys. 16 (2002) 205.
[2] C. Arpesella, et al.Borexino Collaboration, Phys. Lett. B 658 (2008) 101.
[3] H. Back, et al.Borexino Collaboration, Phys. Rev. C 74 (2006) 045805.
[4] H. Back, et al.Borexino Collaboration, Phys. Lett. B 525 (2002) 29.
[5] H. Back, et al.Borexino Collaboration, Phys. Lett. B 563 (2003) 23.
[6] C. Arpesella, et al.Borexino Collaboration, Astropart. Phys. 18 (2002) 1.
[7] C. Arpesella, Borexino Collaboration, et al., Phys. Rev. Lett. 101 (2008) 091302.
[8] M. Chen, et al., Nucl. Instr. and Meth. A 420 (1999) 189.
[9] G. Alimonti, et al.Borexino Collaboration, Astropart. Phys. 8 (1998) 141.
[10] G. Alimonti, et al.Borexino Collaboration, Nucl. Instr. and Meth. A 406 (1998) 411.
[11] J. Benziger, et al., Nucl. Instr. and Meth. A 582 (2007) 509.
[12] F. Gatti, et al., Nucl. Instr. and Meth. A 370 (1996) 609.
[13] F. Elisei, et al., Nucl. Instr. and Meth. A 400 (1997) 53.
[14] G. Alimonti, et al.Borexino Collaboration, Nucl. Instr. and Meth. A 440 (2000) 360.
[15] G. Ranucci, A. Goretti, P. Lombardi, Nucl. Instr. and Meth. A 412 (1998) 374.
[16] D. Manuzio, Towards the detection of submev solar neutrinos in Borexino: data reconstruction and analysis tools, Ph.D. Thesis, Università di Genova, 2004.
[17] A. Pocar, AIP Conf. Proc. 785 (2005) 153.
[18] G. Zuzel, et al., Nucl. Instr. and Meth. A 498 (2003) 240.
[19] M. Wojcik, G. Zuzel, Nucl. Instr. and Meth. A 524 (2004) 355.
[20] A. Pocar, Low background techniques and experimental challenges for Borexino and its nylon vessels, Ph.D. Thesis, Princeton University, 2003.
[21] L. Cadonati, The Borexino solar neutrino experiment and its scintillator containment vessel, Ph.D. Thesis, Princeton University, 2003.
[22] K. McCarty, The Borexino nylon film and the third counting test facility, Ph.D. Thesis, Princeton University, 2006.
[23] A. Ianni, et al., Nucl. Instr. and Meth. A 537 (2005) 683.
[24] A. Brigatti, et al., Nucl. Instr. and Meth. A 537 (2005) 521.
[25] L. Oberauer, et al., Nucl. Instr. and Meth. A 530 (2004) 453.
[26] R. Cavaletti, et al., Nucl. Instr. and Meth. A 324 (1993) 580.

[27] G. Ranucci, et al., Nucl. Instr. and Meth. A 330 (1993) 276.
[28] G. Ranucci, et al., Nucl. Instr. and Meth. A 333 (1993) 553.
[29] G. Ranucci, et al., Nucl. Instr. and Meth. A 337 (1993) 211.
[30] B. Caccianiga, et al., Nucl. Instr. and Meth. A 496 (2003) 353.
[31] O.Yu. Smirnov, Instr. Exp. Tech. 45 (3) (2002) 363.
[32] R. Dossi, et al., Nucl. Instr. and Meth. A 451 (2000) 623.
[33] O.Yu. Smirnov, et al., Instr. Exp. Tech. 47 (1) (2004) 69.
[34] V. Lagomarsino, G. Testera, Nucl. Instr. and Meth. A 430 (1999) 435.
[35] F. Gatti, et al., Nucl. Instr. and Meth. A 461 (2001) 474.
[36] C. Lendvai, Identification of muon-induced signals in the deep underground neutrino-scintillation-detector Borexino, Ph.D. Thesis, Technische Universität München, 2005.
[37] D. D'Angelo, Towards the detection of submev solar neutrinos in Borexino: data readout, data reconstruction and background identification, Ph.D. Thesis, Technische Universität München, 2006.
[38] A. Razeto, Events readout for a real-time neutrino detector, Ph.D. Thesis, Università di Genova, 2002.
[39] G. Ranucci, et al., IEEE Trans. Nucl. Sci. NS-51 (2004) 1784.
[40] J. Boger, et al.SNO Collaboration, Nucl. Instr. and Meth. A 449 (2000) 172.
[41] A. Athanassopoulos, et al.LNSD collaboration, Nucl. Instr. and Meth. A 388 (1997) 149.
[42] M. Apollonio, et al.CHOOZ collaboration, Phys. Lett. B 420 (1998) 397.
[43] J. Maneira, Calibration and monitoring for the Borexino solar neutrino experiment, Ph.D. Thesis, Lisbon University, 2001.
[44] H. Simgen, G. Zuzel, Ultrapure gases—from the production plant to the laboratory, in: P. Loaiza (Ed.), AIP Conference Proceedings, vol. 897, Topical Workshop on Low Radioactivity Techniques: LRT 2006, Aussois, France, Springer, Berlin, 2007, p. 45.
[45] H.O. Back, Internal radioactive source calibration of the Borexino solar neutrino experiment, Ph.D. Thesis, Virginia Polytechnic Institute and State University, 2004.
[46] M.E. Monzani, Characterization and calibration of the borexino detector for solar and supernova neutrinos, Ph.D. Thesis, Università di Milano, 2005.
[47] J.B. Birks, Photophysics of Aromatic Molecules, Wiley-Interscience, London, 1970.
[48] E. Gatti, F. De Martini, Nucl. Electronics, vol. 2, IAEA, Wien, 1962, p. 265.
[49] D. Franco, The Borexino experiment: test of the purification systems and data analysis in the counting test facility, Ph.D. Thesis, Università di Milano, 2005.
[50] G. Alimonti, et al.Borexino Collaboration, Eur. Phys. J. C 47 (2006) 21.